

Utah State University

DigitalCommons@USU

All Graduate Theses and Dissertations

Graduate Studies

5-2016

Throttleable GOX/ABS Launch Assist Hybrid Rocket Motor for Small Scale Air Launch Platform

Zachary S. Spurrier
Utah State University

Follow this and additional works at: <https://digitalcommons.usu.edu/etd>

 Part of the [Aerospace Engineering Commons](#), and the [Mechanical Engineering Commons](#)

Recommended Citation

Spurrier, Zachary S., "Throttleable GOX/ABS Launch Assist Hybrid Rocket Motor for Small Scale Air Launch Platform" (2016). *All Graduate Theses and Dissertations*. 5020.

<https://digitalcommons.usu.edu/etd/5020>

This Thesis is brought to you for free and open access by the Graduate Studies at DigitalCommons@USU. It has been accepted for inclusion in All Graduate Theses and Dissertations by an authorized administrator of DigitalCommons@USU. For more information, please contact digitalcommons@usu.edu.



THROTTLEABLE GOX/ABS LAUNCH ASSIST HYBRID ROCKET MOTOR
FOR SMALL SCALE AIR LAUNCH PLATFORM

by

Zachary S. Spurrier

A thesis submitted in partial fulfillment
of the requirements for the degree

of

MASTER OF SCIENCE

in

Aerospace Engineering

Approved:

Stephen Whitmore, Ph.D.
Major Professor

Rees Fullmer, Ph.D.
Committee Member

David Geller, Ph.D.
Committee Member

Ling Liu, Ph.D.
Outside Member

Mark R. McLellan, Ph.D.
Vice President for Research and
Dean of the School of Graduate Studies

UTAH STATE UNIVERSITY
Logan, Utah

2016

Copyright © Zachary S Spurrier 2016

All Rights Reserved

ABSTRACT

Throttleable GOX/ABS Launch Assist Hybrid Rocket Motor
for Small Scale Air Launch Platform

by

Zachary S. Spurrier, Master of Science
Utah State University, 2016

Major Professor: Dr. Stephen A. Whitmore
Department: Mechanical and Aerospace Engineering

Aircraft-based space-launch platforms allow operational flexibility and offer the potential for significant propellant savings for small-to-medium orbital payloads. The NASA Armstrong Flight Research Center's Towed Glider Air-Launch System (TGALS) is a small-scale flight research project investigating the feasibility for a remotely-piloted, towed, glider system to act as a versatile air launch platform for nano-scale satellites. Removing the crew from the launch vehicle means that the system does not have to be human rated, and offers a potential for considerable cost savings. Utah State University is developing a small throttled launch-assist system for the TGALS platform. This "stage zero" design allows the TGALS platform to achieve the required flight path angle for the launch point, a condition that the TGALS cannot achieve without external propulsion. Throttling is required in order to achieve and sustain the proper launch attitude without structurally overloading the airframe. The hybrid rocket system employs gaseous-oxygen and acrylonitrile butadiene styrene (ABS) as propellants. This thesis summarizes the development and testing campaign, and presents results from the clean-sheet design

through ground-based static fire testing. Development of the closed-loop throttle control system is presented.

PUBLIC ABSTRACT

Throttleable GOX/ABS Launch Assist Hybrid Rocket Motor
for Small Scale Air Launch Platform

Zachary S. Spurrier

The ability for an aircraft-based launch platform to place an orbital payload onto a nominal launch trajectory at a higher energy state -- altitude, velocity, flight path angle, and azimuth --using highly-efficient air breathing propulsion instead of a much lower-efficiency rocket system, offers the potential for a significantly smaller launch vehicle. An airborne platform also provides the ability to launch from multiple locations and allows for significantly increased "system responsiveness." The NASA Armstrong Flight Research Center's Towed Glider Air-Launch System (TGALS) is a small-scale flight research project investigating the feasibility for a remotely-piloted, towed, glider system to act as a versatile air launch platform for nano-scale satellites. Removing the crew from the launch vehicle means that the system does not have to be human rated, and offers a potential for considerable cost savings. A small throttled "stage zero" rocket system is being designed to allow the TGALS platform to achieve the required launch point flight path angle, a condition that the TGALS cannot achieve without external propulsion. Throttling is required in order to achieve and sustain the proper launch attitude without structurally overloading the airframe. A hybrid rocket motor using gaseous oxygen and a solid ABS fuel as propellants was chosen for this project due to the inherent "green" and safe nature of the propellants. This thesis summarizes the development and testing

campaign, and presents results from the clean-sheet design through ground-based static fire testing. Development of the closed-loop throttle control system is presented. The throttle control system uses chamber pressure as a system feedback and throttle control is actuated through an actively modulated ball valve that restricts the oxidizer flow into the system. Presented ground test results demonstrate that the throttle control system was able to follow the thrust profile in a predictable manner, allowing for a repeatable throttle response to a pilot-prescribed input command.

ACKNOWLEDGEMENTS

I would like to express my most sincere gratitude to Dr. Stephen Whitmore for allowing me to be a part of the hybrid propulsion research team at Utah State University, and for all of his help and guidance on this project. I would also like to thank Sean Walker for all of his help in designing and building the necessary hardware for this project, and for his constant support and assistance during testing. Additionally, I would like to thank my family for their unwavering support and belief in me while I finished my degree. I would also like to thank Stephen Merkley and Dan Merkley for always being willing to help me troubleshoot problems, and for all of their help along the way.

Zee Spurrier

CONTENTS

ABSTRACT.....	iii
PUBLIC ABSTRACT	v
ACKNOWLEDGEMENTS	vii
CONTENTS.....	viii
LIST OF TABLES	x
LIST OF FIGURES	xi
ACRONYMS.....	xiii
NOMENCLATURE	xv
1 INTRODUCTION	1
1.1 Advantages of Hybrid Rocket Motors for the Launch Assist Motor.....	4
1.2 Issues Associated with Hybrid Rocket Motors.....	6
1.3 Additive Manufacturing Solutions to Existing Hybrid Propulsion Disadvantages	8
1.4.1 Additive Manufacturing of Hybrid Propellants.....	8
1.4.2 Regression Rate Enhancement Using Helical Fuel Port Structures	9
1.4.3 Arc-Ignition of FDM-Processed ABS Fuel Grains	9
1.4 Throttleable Hybrid Literature Review.....	10
2 RESEARCH OBJECTIVES	15
2.1 Cold Flow Valve Characterization.....	16
2.2 Static Hot Fire System Characterization.....	16
2.3 Short Duration Closed Loop Hot Fire Tests	17
2.4 Simulation Development	17
2.5 Full Length Throttle Following / Closed Loop Sim Verification.....	17
3 SYSTEM DESIGN	19
3.1 Hybrid Motor Combustion Chamber and Ignition System.....	19
3.2 Flight Test Oxidizer Delivery System	23
3.3 Ignition System Power Processing Unit and Control System.....	25

3.4	Ground Test System Overview	26
4	TESTING AND EVALUATION	28
4.1	Cold Flow Valve Characterization.....	28
4.2	Cylindrical Port Hot Fire Tests	31
4.3	Measuring the Required Regulator Set Point.....	35
4.4	Oxidizer-to-Fuel Ratio for the Helical Fuel Port	37
4.5	Throttle Curve Evaluation.....	39
4.6	Closed Loop Throttle Testing	41
4.7	Closed Loop Throttle Filter Tuning.....	43
4.8	Closed Loop Throttle Following Tests	46
4.9	Commanded Thrust Profile to Response Transfer Function.....	47
	CONCLUSION.....	49
	REFERENCES	52

LIST OF TABLES

Table	Page
1. Thrust Chamber Component Dimensions and Weights.....	24

LIST OF FIGURES

Figure	Page
1. CONOPS of Towed-Glider Air Launch System.....	2
2. Demonstration Prototype of Towed-Air Launch Platform	3
3. Top-Level Schematic of LAPU Hybrid Motor System Components.	19
4. LAPU Hybrid Motor with Snap-Together Helical Segments.....	21
5. Flight Vehicle P&ID.	22
6. Installed LAPU System Schematic.....	22
7. Schematic of the Ultravolt HVPS System Pinouts and Interface.	25
8. Launch-Assist Motor Ground Systems P&ID.	26
9. Ground Test Cart for TGALS LAPU Verification Testing.	27
10. Cold Flow Sweep Mass Flow Data.....	29
11. Static Throttle Position Results.....	30
12. Regression Rate for GOX/ABS Cylindrical Port Tests.	33
13. Oxidizer-to-Fuel Shift of Cylindrical ABS Fuel Port.	34
14. Regulator Droop as a Function of Oxidizer Mass Flow, Set Point.....	36
15. Full Throttle Thrust Chamber Pressure, and Thrust Coefficient as a Function of Regulator Set Point.	36
16. Achieved O/F Range for Helical Fuel Port Burn at Near Full Throttle and the resulting Effect on C*.	37
17. Cstar, Combustion Efficiency, and Isp as a Function of Burn Time.	38
18. Helical Motor Response as Function of.....	40
19. Combustion Efficiency as a Function of Throttle Command.	40
20. Specific Impulse as a Function of Throttle Command.	41
21. Proportional Closed-Loop Controller Layout.	42
22. Thrust Profiles for Various Closed-Loop Step Tests.....	42
23. Finding the Best Fit Transfer Function Parameters.	44
24. Simulation Matching for Full Length Hot-Fire Test.....	45

25. Sample Controller Tuning Simulation Runs.....	46
26. Verification Push-up Pull-over Thrust Profile.....	47
27. Best Fit Transfer Function Commanded Thrust to Measured Thrust.....	48

ACRONYMS

ABS	acrylonitrile butadiene styrene
AMROC	American Rocket Company
AP	ammonium perchlorate
CEA	Chemical Equilibrium with Applications
CONOPS	concept of operations
FDM	fused deposition modeling
FLOX	oxygen difluoride
GOX	gaseous oxygen
HAST	High Altitude Supersonic Target
HERO	hazards of electromagnetic radiation
HTPB	hydroxyl-terminated polybutadiene
HVPS	high voltage power supply
HYSR	hybrid sounding rocket
JIRAD	Joint Government/Industry Research and Development
KTAs	knots true air speed
LAPU	launch-assist propulsion unit
LEX	Lithergol Experimental
LOX	liquid oxygen
MSL	mean sea level
N_2O	nitrous oxide
P&ID	pipng and instrumentation diagram
PMM	polymethylmethacrylate
PPU	power processing unit
RSRM	reusable solid rocket motor
TFTA	tetraformaltrisazine
TGALS	Towed Glider Air-Launch System
TTL	transistor-transistor logic

UALR	University of Arkansas at Little Rock
USB	universal serial bus
USU	Utah State University
UTC	United Technology Center

NOMENCLATURE

A^*	nozzle area
A_1	venturi inlet area
A_2	venturi throat area
A_c	cross sectional port area
a	scale factor
C^*	characteristic Velocity
C_d	discharge coefficient
c_v	flow coefficient
G_{ox}	oxidizer mass flux
I_{sp}	specific impulse
k_p	proportional gain
L	fuel port length
M_w	molecular weight
$\%MVT$	percentage max valve travel
\dot{m}	mass flow rate
\dot{m}_{ch}	choking mass flow
m	burn exponent
n	burn exponent
P_0	combustion chamber pressure
R_g	specific gas constant
R_u	universal gas constant
\dot{r}_L	longitudinal regression rate
T_0	stagnation temperature
\dot{m}	mass flow rate
O/F	oxidizer to fuel mass flow ratio
p	pressure

Q	volumetric flow rate
γ	heat capacity ratio
ζ_1	combined actuator/ball valve damping ratio
ζ_2	ballistics model damping ratio
η^*	combustion efficiency
ρ	density
τ_1	actuator/ball valve time latency
τ_2	ballistics model time latency
ω_1	actuator/ball valve natural response frequency
ω_p	filter cutoff frequency

CHAPTER 1

INTRODUCTION

Since the early days of spaceflight an unachieved goal has been to create an orbital launch system capable of operating from runways with convenience and flexibility similar to aircraft. Due mainly to propulsion technology limitations with chemical rocket engines, nearly all launch systems developed to date perform takeoff vertically from specialized launch pads and have very limited operational flexibility. Fixed-base launches are restricted to certain azimuths and orbit inclinations (depending on launch site) and launch windows are typically short in duration and infrequent in occurrence.

A recent NASA-DARPA study [1] has concluded that there exists a significant potential for horizontal air-launch to provide critical strategic advantages and "assured" access to space when compared to fixed base launch operations. Because the launch altitude and airspeed are achieved using a high-efficiency air-breathing propulsion system, there is a significant reduction in the required ΔV that must be delivered by the launch vehicle, and a significantly smaller launch vehicle is allowed. The study concludes that a performance boost to orbit of 50% may be obtainable. An air launched vehicle can also achieve a wide range launch inclinations and right ascensions from a single deployment site. Launches performed at or near the equator can be accomplished with a 12% to 25% reduction in propellant mass. More importantly, air-launch provides a wide range of operational options including on-demand launch azimuth, flexible launch windows, and nearly all-weather launch opportunities. This capability enhancement can lead to increased launch rates and an associated overall launch-cost reduction.

The DARPA/NASA study concluded that a towed, remotely-piloted, unpowered glider bottom-launching a space-launch vehicle has the potential to be significantly smaller and operationally cheaper than a dedicated human crewed carrier aircraft. Because the towed platform is separated from the launch vehicle by a significant distance, the risk to human crew is significantly reduced. Consequently, the launch platform does not require human flight certification.

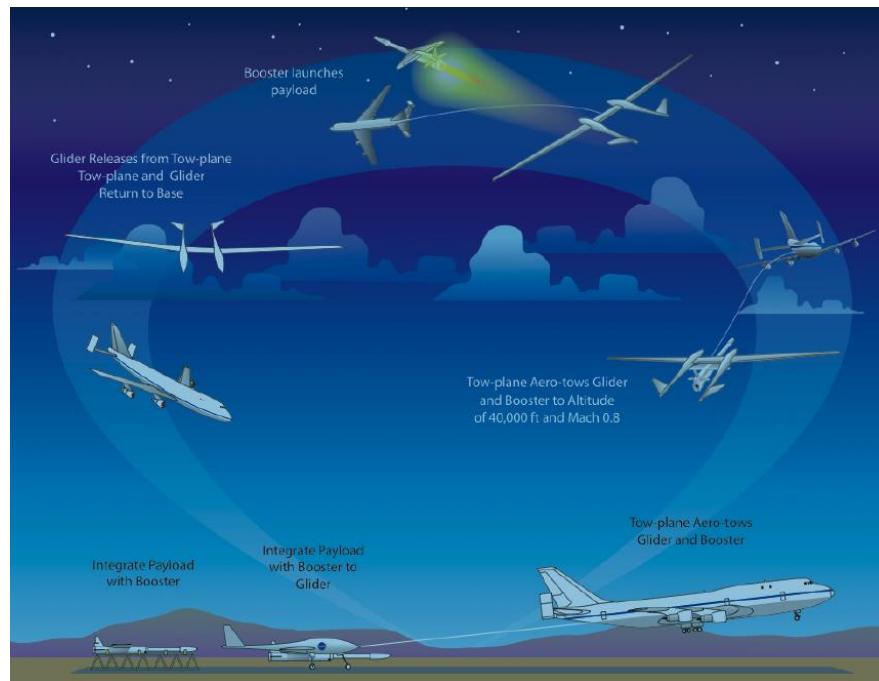


Figure 1. CONOPS of Towed-Glider Air Launch System.

The high lift to drag towed platform offers the potential for a significantly increased operational range when compared to a coupled launch vehicle and lift platform. Finally, the glider platform can be towed to the launch altitude using a variety of options, this

concept offers a significant increase in operational flexibility. These features offer the potential to dramatically lower launch operating costs. Such cost savings could represent a market-disruptive potential for the emerging commercial spaceflight industry. Figure 1 shows the Concept of Operations (CONOPS) for a TGALS operational platform.

Previous air-launch studies [2,3,4] have demonstrated that a key parameter for optimal air launch trajectories is the launch flight path angle. Conceptually, an optimal air launch flight path angle at the launch altitude and airspeed would place the launch vehicle onto the trajectory follows the optimal ground launch trajectory. The glider platform itself is unable to achieve this flight condition, and launch assist propulsion is required. Currently, AFRC is developing a prototype platform to verify the operational feasibility of the towed-launch platform concept. A primary objective of this demonstration project is to tow to altitude, release, and safely return to base with an instrumented, sub-scale, remotely piloted, twin-fuselage glider with a representative scaled small-rocket system. Figure 2 shows a photograph of the demonstration vehicle scaled-prototype.



Figure 2. Demonstration Prototype of Towed-Air Launch Platform

The launch assist motor is attached to the center-pylon of the launch platform. This demonstration project will allow AFRC to gain operational experience with the towed glider platform, understand aerodynamic and structural interactions of the rocket and pylon, and demonstrate that the launch platform can achieve the proper launch attitude and perform the desired flight maneuver.

Multiple options are available to achieve the required launch-assist total impulse, including a small solid rocket booster, a bi-propellant liquid system, a cold-gas system, a mono-propellant hydrazine system, and a hybrid rocket system. The bi-propellant liquid rocket was discarded due to the associated complexity and expense of engineering the required sub-systems. The hydrazine system was discarded because of the potential vapor hazard and the associated operational complexities of working with a toxic propellant. The solid rocket booster, although offering a simple solution, does not deliver the impulse precision and variable thrust required to place the launch platform onto the proper launch attitude. Finally, because of the associated low specific impulse (I_{sp}), the cold gas system required more propellant than can be carried by the launch platform with the launch vehicle payload. Thus, by process of elimination a hybrid system was selected for the launch-assist propulsion unit (LAPU).

1.1 Advantages of Hybrid Rocket Motors for the Launch Assist Motor

When compared to other commonly used rocket systems such as solid and liquid motors, hybrid rocket motors tend to come out ahead on environmental friendliness, operational safety and versatility. [5] Due to the fact that the oxidizer and fuel

components are kept separately, and by themselves are generally non-explosive, hybrid rocket motors can be safely handled and transported with minimal preparation.

When compared to conventional liquid- and solid-propelled rocket systems, hybrid rockets -- where the propellants typically consist of a benign liquid or gaseous oxidizer and an inert solid fuel -- possess well-known operational safety and handling-advantages. A study by the U.S. Department of Transportation [5] concluded that hybrid rocket motors can be safely stored and operated without a significant risk of explosion or detonation, and offer the potential to significantly reduce operating costs for commercial launch vehicles.

Additionally, hybrid rockets have the benefit in ease of throttleability, requiring as little as a single throttle valve on the oxidizer feed line. Liquid motors also have the benefit of throttleability, but the propellants used are generally hydrazine or hydrogen peroxide monopropellants, or monomethyl hydrazine and nitrogen tetroxide. [6] These liquid propellants are quite dangerous to the environment and the people who work around these propellants. They are also more prone to sudden decomposition and explosions from shock or contamination.

The trade off when selecting a hybrid rocket motor is that they tend to deliver a lower specific impulse (I_{sp}). The benefits on cost and safety, as well as the need for a “smart stage” are the reasons why a hybrid rocket motor can be advantageous. For this project a gaseous oxygen (GOX) and acrylonitrile butadiene styrene (ABS) motor are used. The benefits of using gaseous oxygen as the oxidizer is you can’t really get a better oxidizer than straight oxygen, and it is a relatively safe oxidizer to work around. However, there

comes a tradeoff in the fact that even at high pressure levels gaseous oxygen isn't very dense. This means there is a lot of weight in the tanks to hold the oxidizer that is just dead weight on the vehicle. While GOX is sufficient for this project, it may be desirable to choose a liquid oxidizer that is more volumetrically efficient for in space thrusters, or for future projects.

1.2 Issues Associated with Hybrid Rocket Motors

In spite of these above-mentioned well-known safety and handling advantages; conventionally-designed hybrid rocket systems have not seen widespread commercial use due to several key drawbacks that exist with conventional hybrid-system designs. First, the internal motor ballistics of hybrid combustion produce fuel regression rates typically 25-30% lower than solid fuel motors in the same thrust and impulse class. [7] These lowered fuel regression rates tend to produce unacceptably high oxidizer-to-fuel (O/F) ratios that lead to combustion instability, erosive burning, nozzle erosion, and reduced motor duty cycles. To achieve O/F ratios that produce acceptable combustion characteristics, traditional cylindrical fuel ports have been fabricated with very long length-to-diameter ratios. This high aspect ratio results in poor volumetric efficiency that is incompatible with small spacecraft applications.

Second, because of the relative propellant stability, hybrid rocket systems can be difficult to ignite; and a substantial ignition enthalpy source is required. The ignition source must provide sufficient heat to pyrolyze the solid fuel grain at the head end of the motor, while simultaneously providing sufficient residual energy to overcome the activation energy of the propellants. Such high-energy devices often come with a suite of

environmental and objectives risks, and operational challenges.

Most conventional hybrid rocket applications have used high output pyrotechnic or “squib” charges to initiate combustion. Pyrotechnic charges are extremely susceptible to the Hazards of Electromagnetic Radiation to Ordnance (HERO), [8] and large pyrotechnic charges present a significant explosion hazard that is incompatible with rideshare opportunities. Most importantly, for nearly all applications pyrotechnic ignitors are designed as "one-shot" devices that do not allow a multiple restart capability. Thus the great potential for re-startable upper stages or in-space maneuvering systems using hybrid propulsion remains largely unrealized. An operational hybrid system with multiple restart capability does not currently exist.

Finally, the "cast and cure" methods for producing conventional thermosetting hybrid fuel grain materials including Hydroxyl-Terminated Polybutadiene (*HTPB*), Polybutadiene Acrylonitrile (*PBAN*), and Glycidyl Azide Polymer (*GAP*) are necessarily labor intensive, and high production rates cannot be achieved without a significant manufacturing infrastructure. These binder materials are mixed from liquid base-components, degassed under vacuum, and then cast and cured in a fuel grain mold. This labor intensive manufacture and assembly approach results in market prohibitive production costs and cannot produce the numbers and varieties of motors required to support the what is expected to be a fast-growing commercial space industry.

The isocyanate-based materials used to cure these previously described fuel polymers present a wide variety of Environmental Safety and Occupational Health (ESOH) risks including carcinogenic and detrimental reproductive effects. The US Department of

Defense considers these materials to be environmentally unsustainable for large-scale propellant production, and is actively seeking replacement alternatives. [9]

1.3 Additive Manufacturing Solutions to Existing Hybrid Propulsion Disadvantages

Whitmore, and Peterson [10] have recently investigated the use of additively-manufactured Acrylonitrile Butadiene Styrene (ABS) thermoplastic as a hybrid rocket fuel material. A key outcome of this research was the demonstrated thermodynamic equivalence of ABS to the conventional hybrid rocket fuel HTPB when burned with nitrous oxide (N_2O). ABS achieved specific impulse and characteristic velocity that are nearly identical to HTPB. ABS and HTPB fuel regression mass flow rates for cylindrical fuel ports were measured to be nearly identical.

When compared to HTPB, however, ABS has several mechanical properties that make it very attractive as a hybrid rocket fuel. ABS is an inexpensive thermoplastic material that is widely mass-produced for a variety of non-combustion applications including household plumbing and structural materials. ABS is a non-crystalline material with an amorphous structure. As such ABS does not possess a true melting point, but exists in a highly "softened" semi-fluid state before vaporizing. This fluid state exists over a wide temperature range.

1.4.1 Additive Manufacturing of Hybrid Propellants

This melting property makes ABS the material of choice for a modern form of additive manufacturing known as Fused Deposition Modeling (FDM). In FDM, a plastic filament is unwound from a coil and supplies material to an extrusion nozzle. The nozzle is heated to melt the material and can move in both the horizontal and vertical directions

by a computer numerically controlled (CNC) mechanism. Identical pieces can be produced simultaneously by multiple vendors using a well-developed commercial technology.

1.4.2 Regression Rate Enhancement Using Helical Fuel Port Structures

Exploiting the FDM fabrication process for ABS offers the potential to revolutionize the manufacture of hybrid rocket fuel grains. FDM can support high production rates and offers the potential of improving hybrid fuel grain quality, consistency, and performance, while reducing development and production costs. These manufacturing advantages are not achievable using the conventional methods of solid propellant production.

Using additive manufacturing hybrid fuel grains can be fabricated with an almost infinite range of fuel port shapes, allowing for significant enhancement of burn properties and combustion efficiencies. Of particular interest are helical fuel structures whose centrifugal flow patterns have been shown to significantly increase the fuel regression rate. Regression rate amplification factors exceeding 3.0 have been demonstrated. [11]

1.4.3 Arc-Ignition of FDM-Processed ABS Fuel Grains

Finally, FDM-processed ABS possesses unique electrical breakdown properties that can be exploited to allow for rapid on-demand system ignition. [12] This technology derives from the unique electrical breakdown properties of 3-D printed acrylonitrile butadiene styrene (ABS), discovered serendipitously while investigating the thermodynamic performance of ABS as a hybrid rocket fuel. Additive manufacturing is an essential feature of this concept. The layering of the printed ABS creates very small radius surface features. When electrodes are embedded into the system and voltage is

applied across the electrodes, these features concentrate charge at many discrete points on the material surface and allow a strong electrical arc to occur at moderate voltage levels. The electric field generated by the arc produces joule level heating and results in pyrolysis along the conduction path. When this pyrolysis concurrently occurs with oxidizer flow into the combustor, there exists a mixture of combustible gaseous and a source of activation energy (provided by the arc). This combination rapidly leads to self-sustaining combustion along the entire fuel port surface. Identical ABS fuel segments made from extruded/machined ABS do not exhibit these moderate voltage arcing properties.

This concept has been developed into a power-efficient system that can be started and restarted with a high degree of reliability. This prototype system, when fully developed, could become a "drop in" replacement for hydrazine thrusters for a variety of space propulsion applications. Multiple prototype devices based on this concept with thrust values ranging from 4.5 to 900 N have been developed and tested. All units are capable of multiple restarts and can be operated in either continuous or pulse modes. The 900 N thruster system described by Ref. [12] form the basis for the launch assist motor developed by this research campaign.

1.4 Throttleable Hybrid Literature Review

One of the earliest recorded throttled hybrids belongs to G. Moore and K. Berman from General Electric, developed in the late 1940's. [13] This system started out as an augmented monopropellant hydrogen peroxide motor to which a polyethylene fuel grain section was added to increase specific impulse, I_{sp} . They noted that throttling was easily

accomplished through the use of a single valve, but that due to the thermal instabilities of peroxide it was difficult to vary the burn rate by more than a factor of two.

In the 1960's ONERA developed a throttled hybrid based around hypergolic propellant combination of red fuming nitric acid and an amine fuel of meta toluene diamine/nylon propellant combination. [14] These tests made up the Lithergol Experimental (LEX) tests. This motor was shown to have the ability to throttle over a 5/1 range from 10kN to 2 kN utilizing an air driven solenoid valve with a programmable timer. During the same time period United Technology Center and Beech Aircraft were working on the Sandpiper, a target drone under development for the Air Force. The motor for Sandpiper used a nitric oxide and nitrogen peroxide oxidizer (RON-25), and a polymethylmethacrylate (PMM) and magnesium fuel. Sandpiper was shown to be throttleable over an 8/1 range from a peak thrust of 2.3 kN. [15,16] To achieve this throttle, Sandpiper had two oxidizer feed lines, one that had a preset flow control valve that provided enough oxidizer for the vehicle to maintained a constant velocity, and a second valve which allowed the motor to accelerate. The second valve was closed once cruise velocity had been reached.

Another Air Force project at this time was the High Altitude Supersonic Target (HAST), which, in comparison to Sandpiper, had a larger thrust chamber, IRFNA-PB/PMM fuel, cruciform port configuration, and the oxidizer was pressurized by ram air turbine instead of a nitrogen top pressure. [17] The HAST motor had a peak thrust of 5.3kN with a 10/1 throttle range controlled by an on command throttling valve consisting of a torque motor with a ball screw that actuated a pintle valve. In flight the HAST

motors were programmed to throttle from 50% to 100% over 20 seconds. After this point, the valve position could be manually adjusted remotely.

One of the companies that worked on Sandpiper was United Technology Center (UTC). They also worked on a hybrid propulsion system designed for use in tactical missiles. [18] This system used dual oxidizer lines with separate solenoids, one running to a sustain manifold, and one to a boost manifold. This allowed the motor to be throttled between high thrust at 22.2 kN, and cruise thrust at 11.1 kN. This motor was restartable, and used a fuel combination of boron, tetraformaltrisazine (TFTA), ammonium perchlorate (AP) and hydroxyl-terminated polybutadiene (HTPB) known as HFX 7808 with chlorine pentafluoride (ClF_5) as the oxidizer. This hybrid system was ground tested. UTC also worked on another hybrid motor that was designed as a vehicle upper stage. [19] This motor was throttleable from 8/1 with a peak thrust of 22.2 kN. This system also only saw ground testing, likely due to the risks of the chosen propellants; oxygen difluoride (FLOX) with a lithium based fuel.

Development of hybrid rocket motors was scarce in the 1970s and early 1980s due primarily to the success of solid and liquid motors of the time. However, the increased need for propulsion on commercial satellites and the catastrophic failures of both the Challenger and a Titan III caused a resurgence in interest in hybrid rocket motors, due to their inherent safety and reduced cost. It was in the 1980s when the American Rocket Company (AMROC) was formed. One of the motors they designed was the H-1500, which was designed to be used in the first two stages of AMROC's Aquila launch vehicle. [20] This 1112 kN thruster was throttled by varying gas driven turbo pumps

which pumped the motor's liquid oxygen (LOX) oxidizer. AMROC also designed the H-30 motor which could be used as Aquila's fourth stage. This motor used an oxidizer of nitrous oxide in a blow-down feed system using a single throttling valve. It was during this time that NASA began the Hybrid Propulsion Technology Program to investigate whether hybrid rocket boosters could provide a safer alternative to the Space Shuttle's Reusable Solid Motor (RSRM) boosters. A large scale motor designed for 4448 kN, and a cluster of four ¼ scale motors were evaluated with various oxidizers and fuels. Two oxidizer delivery systems were developed, one with four individual throttle valves in a pressure fed system, and one with a pump fed system. The pressure fed system was designed for a 1.6/1 throttle ratio, and the pump fed system was designed for 2.4/1 throttle ratio.

NASA started the Joint Government/Industry Research and Development (JIRAD) program in the mid-1990s. [21,22] Two of the hybrid motors evaluated at this time were an 11-inch diameter and a 24-inch diameter motor designed for 13.3 kN and 178 kN thrust respectively. Both of these motors operated in a binary thrust mode like the UTC tactical missile system. LOX or GOX were used as the oxidizers with a fuel of polycyclopentadiene and HTPB known as UTF-29901.

Lockheed Martin and Marshall Space Flight Center started the Hybrid Sounding Rocket (HYSR) project in 1999. Designed to replace multistage sounding rockets with a single stage, HYSR rockets were designed using LOX as the oxidizer with aluminized HTPB as the fuel. [23] This motor had a branched oxidizer line with step throttle abilities similar to the JIRAD motors.

Recently, many academic institutions have also developed their own throttleable hybrid rocket motors. The University of Arkansas at Little Rock (UALR) developed an oxidizer delivery system that can throttle the mass flow of the oxidizer to between 18 and 37 g/s using a Teledyne-Hastings HFC307. [24] Stanford has developed a custom throttling plate for the Peregrine sounding rocket that rotates to control the oxidizer mass flow rate to between 50% and 100%. [25,26] Purdue has demonstrated a throttle-down profile similar to what would be experienced in a powered landing, along with a square wave profile similar to a boost/sustain/boost profile used for a tactical missile flight. [27] This motor was able to throttle with a 10/1 ratio using a Habonim control valve. Peterson at Utah State University (USU) developed an 800 N motor that remained stable down to 12N using an oxidizer of nitrous oxide, and HTPB for fuel.

CHAPTER 2

RESEARCH OBJECTIVES

The objectives of this research are to design, build, and test a throttleable GOX/ABS hybrid rocket motor for use as a “stage 0” launch assist propulsion system. The requirements for the system itself are

- Maximum thrust of 200 lbf
- Capable of throttling from below 20% to 100% thrust
- Provide sufficient throttle control to allow the glider to perform a pull-up to 70-degree flight path angle for a minimum of five seconds, followed by a push over back to horizontal flight. This maneuver will be performed at around 85 knots true air speed (KTAS), and at a height of 4500 ft. above mean sea level (MSL)
- The motor should utilize non-toxic, non-explosive propellants, as well as a non-pyrotechnic ignition system to reduce systematic risk.
- After performing the maneuver, the launch assist system should allow for enough remaining energy for the glider launch platform to return to base. This requires contingency oxidizer and fuel, as well as a restartable ignition system.

In order to achieve the above goals, the plan to meet objectives are

- Design analysis from the motor ballistics model to select proper pneumatic system components that will allow enough oxidizer to flow for enough time to meet mission objectives.
- Procurement and fabrication of selected components.
- Cold flow throttle valve characterization tests to determine throttle range of the ball valve actuator
- Static hot fire characterization tests to determine thrust levels at various ball valve set points

- Initial, short closed loop control tests to develop a system simulation which can be used to predict the system's behavior.
- Using the simulation, determine controller parameters that will allow the mission objective to be met.
- Full length pull-up push-over maneuver throttle following tests. Using this test, the system simulation will be refined, and controller parameters can be determined again. Repeat as necessary.
- Once the above criteria have been sufficiently met, closed loop pressure feedback control on a GOX-ABS hybrid rocket motor will have been demonstrated to within satisfactory limits for the mission.

2.1 Cold Flow Valve Characterization

The initial tests performed once the system was built were a series of ball valve sweeps and constant position tests to determine what voltage command corresponded to a ball valve position of full closed and full open. Intermediate values also helped determine how linear the chamber pressure response was in respect to the ball valve position. These tests were required since the ball valve actuator has a range of 270 degrees over the 0-5V input, but the ball valve only requires 90 degrees to go from full closed to full open. More about these tests can be found in section 4.1.

2.2 Static Hot Fire System Characterization

Fixed position hot fire tests were performed in order to determine regulator set point required to meet the 200 lbf thrust level, as well as determine the all necessary ball valve relationships, such as ball valve position to chamber pressure, chamber pressure to thrust, and servo voltage input to oxidizer and fuel mass flow rates. More information about these tests can be found in section 4.2.

2.3 Short Duration Closed Loop Hot Fire Tests

Using the resulting relationships from the static hot fire characterization tests, a proportional closed loop controller was built. The closed loop controller has a low-pass Butterworth filter on the voltage output to the ball valve actuator which acts similarly to an integral term on a typical PI controller. Four tests were performed with arbitrarily selected proportional gains and low pass filter cutoff frequencies to determine what the response of the system was to a 25 to 50% throttle step, as well as to verify that the closed loop controller was behaving as intended. More about the initial closed loop firing test can be found in section 4.3.

2.4 Simulation Development

The measured responses determined from the short duration closed loop hot fire tests were used to determine the transfer function that related the controller command voltage to the system thrust response. Once a satisfactory relationship was found, it became possible to iterate through proportional gain values, as well as cutoff frequencies to predict how the system would respond under various conditions. From there, the desired system response was chosen. The reason this simulation was developed was to remove the need to perform a large number of hot fire tests to find a desirable system response. Thousands of simulated responses could be used, and then verified by a couple of full length hot fire tests instead. More about the development of the simulation can be found in section 2.4.

2.5 Full Length Throttle Following / Closed Loop Sim Verification

The final tests take the best response proportional gain constant, and cutoff frequency value and put it to the test in a closed loop, pressure feedback throttle following

maneuver. This test was considered a success if the measured throttle matched up well with the predicted throttle values from the simulation. Given the small amount of data gathered from the short duration closed loop hot fire tests, it was no big surprise that the simulation didn't quite predict the system response as well as it could have. A total of three full duration closed loop hot fire tests were performed, the first two were used to tune the simulation to better predict system response, and select new proportional gain and cutoff frequency values, and the third test verified that a suitable simulation design and gain values had been chosen. The results of these tests can be found in section 4.7.

CHAPTER 3

SYSTEM DESIGN

Figure 3 presents a top-level solid-model schematic of the Launch Assist Propulsion (LAPU) Systems. The prototype system is based on a previous design tested at Utah State University. [28] Pictured are the gaseous oxygen (GOX) oxidizer tanks, the high pressure fill and relief valves, a tank manifold, a manually-set pressure reducing regulator, a low-pressure burst safety disk, an electronic run-valve, a ball-type throttle valve, an electrical valve actuator, and the motor thrust chamber and pressure case. The associated pneumatic assembly piping and connectors are also shown. Major features are described in detail in the following subsections.

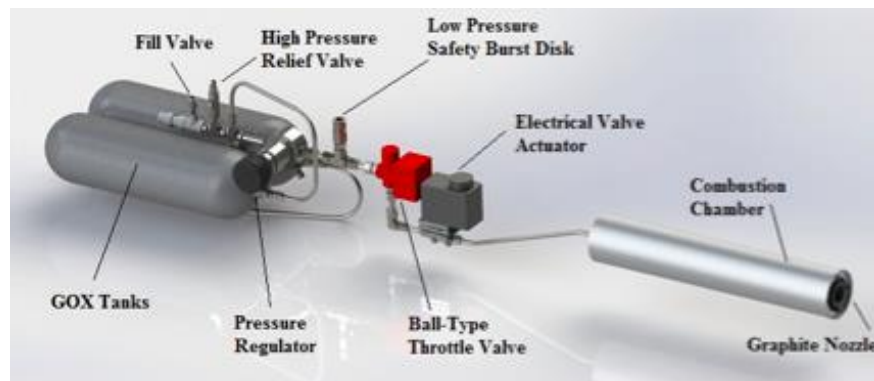


Figure 3. Top-Level Schematic of LAPU Hybrid Motor System Components.

3.1 Hybrid Motor Combustion Chamber and Ignition System.

The hybrid motor system employs gaseous oxygen (*GOX*) as the oxidizing agent and additively-manufactured acrylonitrile butadiene styrene (*ABS*) as the fuel component.

These propellants are non-explosive, non-toxic, and remain inert until combined within the motor combustion chamber and in the presence of an ignition source. The fuel grain is manufactured using the conventional fused deposition modeling (FDM) technique of additive manufacturing for thermoplastics, and features a keyway alignment system that allow the grain segments to be manufactured separately and then assembled for use. The FDM processed grain segments also allow for an embedded helical fuel port that enhances the fuel regression rate and combustion efficiency.

Figure 4 shows a cut-away schematic for the hybrid rocket motor case. Pictured are the helical fuel grain interlocks, injector cap with ignition electrodes, and post-combustion chamber with graphite nozzle insert and adapter. The motor case is constructed from a modified 98 mm Cessaroni solid rocket motor case with an approximate length of 70 cm. The pictured fuel grain is additively manufactured from commercially-available Stratasys ABSplus-340® feed-stock.¹ Table 1 lists dimensions and weights of the major thrust chamber system components.

The system is ignited using a patent pending arc-ignition technology developed at Utah State University. [29] This technology exploits the unique electrical breakdown properties of additively-manufactured ABS to allow on-demand start and restart. The non-pyrotechnic system requires two independent signals to initiate combustion, and is thus dual redundant to the Hazards of Electromagnetic Radiation to Ordnance (HERO) as defined by MIL-STD-464. [30] Figure 4 shows a schematic for the hybrid motor case, the

¹ www.stratasys.com/materials/fdm/absplus/

helical fuel grain interlocks, injector cap with ignition electrodes, and post-combustion chamber with graphite nozzle are shown. The oxidizer injector consists of a single port injector with a $.402 \text{ cm}^2$ area in order to allow the required mass flow of at *least* 250 g/sec (0.55 lbm/sec) into the combustion chamber without choking. The ignition power-processing-unit (PPU) and oxidizer delivery system are not shown in Figure 4. The ground test motor systems are designed to reproduce the flight systems and layout as closely as possible.

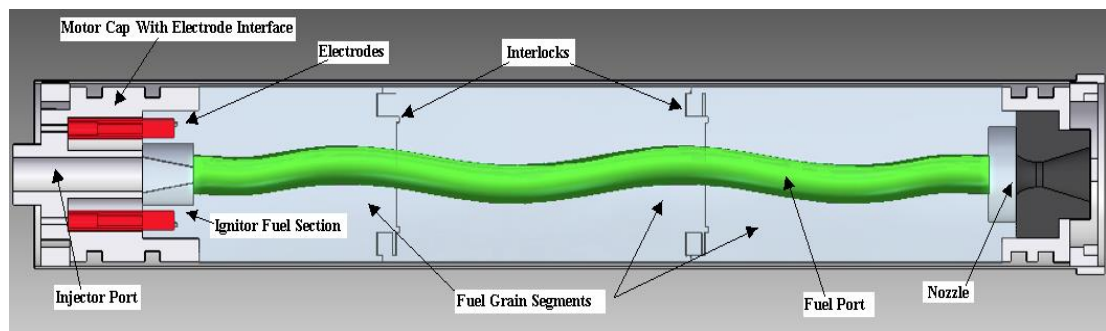


Figure 4. LAPU Hybrid Motor with Snap-Together Helical Segments.

Figure 5 shows the flight system components in the approximate the flight orientation, as mounted to the pylon between the twin vehicle fuselages. The fully loaded system weight is approximately 23.9 kg (52.6 lbm), and is approximately 165 cm (65 in.) in end-to-end length. Each GOX tank is rated for a 4500 psig maximum fill capacity, and holds approximately 1.93 kg (4.24 lbm) of oxidizer when filled at room temperature. The motor dry system weight is approximately 18 kg (40.3 lbm).

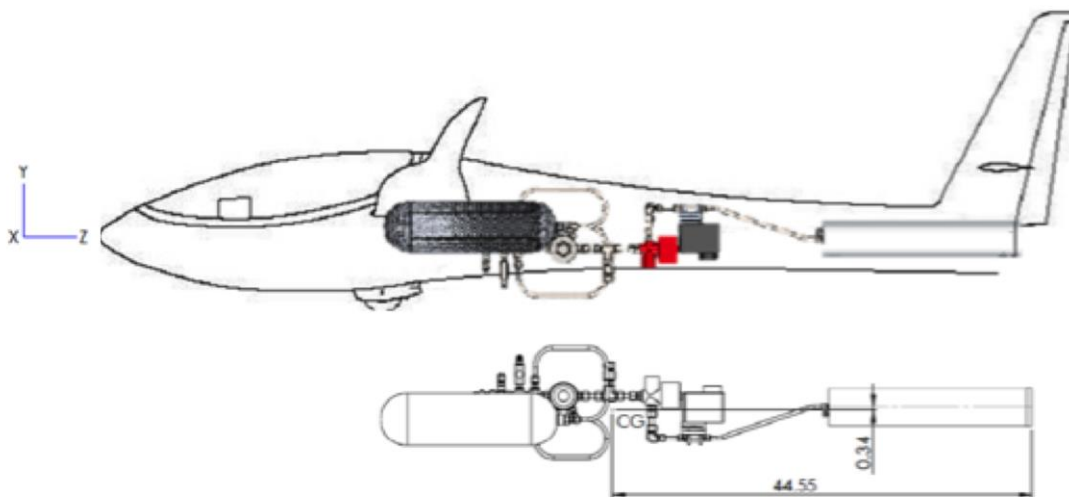


Figure 6. Installed LAPU System Schematic.

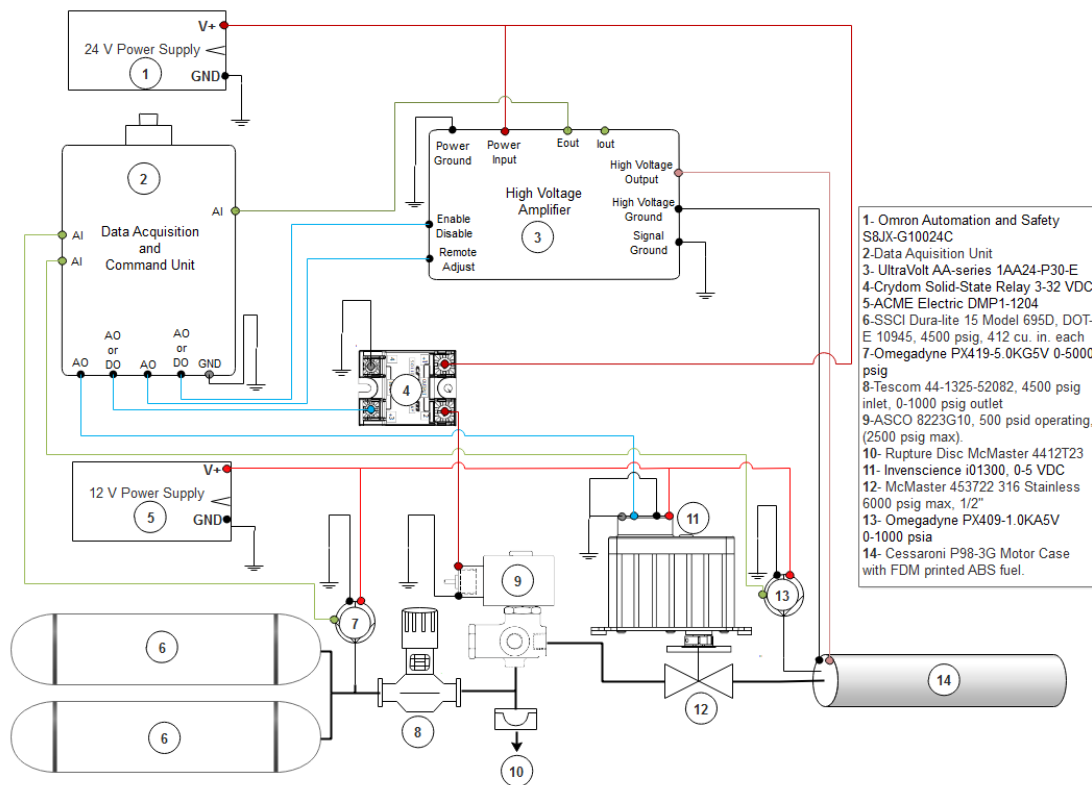


Figure 5. Flight Vehicle P&ID.

3.2 Flight Test Oxidizer Delivery System

Figure 6 presents the oxidizer delivery system piping and instrumentation diagram (P&ID) for the flight test system. The system is designed to operate between 4500-to-1500 psig upstream of the pressure regulator, and between 750-to-800 psig downstream of the regulator. Required safety-of-flight system instrumentation consists of pressure transducers upstream of the regulator and a chamber pressure transducer.

The oxidizer delivery system components consist of

- Two aviation-rated 4500 psig carbon composite gaseous oxygen storage tanks, manifolded together.
- A manual set pressure reducing regulator
- A DC actuated solenoid run valve.
- An electronically actuated servo attached to a 90-degree ball valve
- The thrust chamber injector.

The throttle ball valve allows the system to regulate the mass flow by adjusting the outlet flow coefficient (C_v). A full-open valve C_v range of approximately 2.5 is required to achieve the desired 250 g/sec maximum mass flow level at a valve inlet pressure of approximately 750 psig. The valve is actuated using an *Invensciencei01300* rotary actuator². The 12-V powered ball-valve rotary actuator features 0 to 5 VDC analog input proportional control signal for the full available 0-270 degree actuation.

² http://www.invenscience.com/index_files/torxis_rotary_servo.htm/

The pressure regulator has a lockable, manual set-point. Assuming a full-filled capacity for the O_2 tanks (4500 psig) and the assumed ball-valve C_v (2.5), a regulator set-point range of approximately 750 psia will be required to achieve the prescribed maximum thrust level of approximately 200 lbf. The C_v of the solenoid run valve is 3.0 to ensure that the flow will not choke upstream of the throttling ball valve. The regulator set point had to be manually tuned to adjust for any potential losses in the system run valve. The regulator valve set point of 750 psig was selected to ensure a choking mass flow of greater than 250 g/sec at that pressure set point. Table 1 shows the designed oxidizer and motor components that were selected to meet the mission requirements.

Table 1. Thrust Chamber Component Dimensions and Weights.

Motor Case	Length: 27.73 in. (70.2 cm)	Diameter: 3.86 in. (98 mm)	Empty Weight: 7.95 lbm (3.61 kg)	Total Loaded Motor Weight: 14.41 lbm (6.54 kg)
Injector	Diameter: 0.282 in. (0.716 cm)	Type: Single port, aluminum	Discharge Area: .0623 in ² (.402 cm ²) Cd ~ 0.85	Total Oxidizer Load: 11.2 lbm (3.8 kg)
Machined graphite nozzle	Diameter: 0.728 in. (1.85 cm)	Expansion Ratio: 4.65	Conical exit angle: 15 deg.	Throat Erosion Rate: 0.011 cm/sec
ABS Fuel grain	Length: 23.08 in. (58.61 cm) Diameter: 3.31 in. (8.4 cm)	Initial Port Diameter: 0.9 in. (2.286 cm)	Fuel Weight: 6.462 lbm (2.932 kg)	Helix Ratio: 0.5:1 Pitch Length: 7.69 in. (19.5 cm) (3 turns)

3.3 Ignition System Power Processing Unit and Control System.

The ignition system PPU is based on the UltraVolt® AA-series line of high-voltage power supplies (HVPS). [31] These HVPS units take a 24-28 VDC input and provide a current-limited (30 mA) high voltage output -- up to 1 kV. The output signal is initiated by a commanded TTL-level signal. Units with output capacities from 4-30 watts are available. Previous experience with this ignition system has demonstrated that ignition can be achieved using as little as 6 watts; [32] however, in order to ensure guaranteed reliable motor ignition a 30-watt model will be employed for this design. Figure 7 shows the interface to the AA-series HVPS. The unit features current and high-voltage output signals that are used to monitor the system performance on the flight vehicle. The remote adjust input is set to the maximum value. Figure 8 shows the complete electronics and piping diagram for the ground test system. At this point in the design process, the data acquisition system and flight computer for the flight system have not been selected. For the ground system a USB-based NI cDAQ-9174 is used.

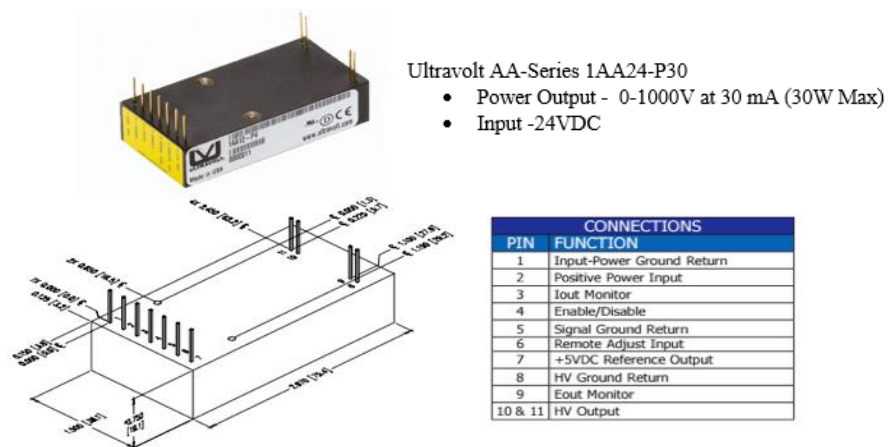


Figure 7. Schematic of the Ultravolt HVPS System Pinouts and Interface.

3.4 Ground Test System Overview

The ground test system used to perform the preliminary integration and qualification tests on the LAPU subsystems employs a more extensive instrumentation suite including an inline custom venturi flow meter on the oxidizer feed line, downstream of the pressure regulator. Additionally, a load cell is used to verify thrust from pressure, and calibrate thrust for a given pressure in the first place. Thermocouples were integrated into the original system, but after safety was verified they were deemed unnecessary. The system is integrated onto a portable test cart with all hot fire testing performed in the Propulsion Research Laboratory's on-campus test cell. Figure 8 shows piping and instrumentations test schematic for the ground system.

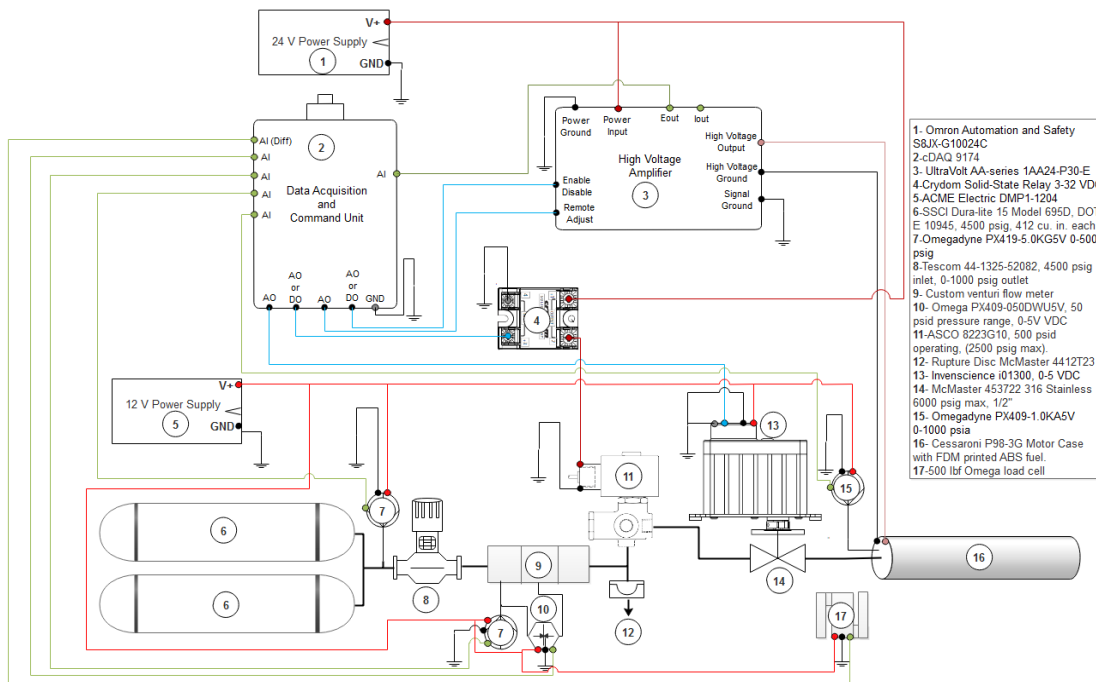


Figure 8. Launch-Assist Motor Ground Systems P&ID.

Figure 9 shows the physical test cart on which the tests were performed. The ground test system is operated using a National Instruments USB-based *NI cDAQ-9174* Data Acquisition and Control Unit³ with data logging and system control performed via a LabVIEW interface program.

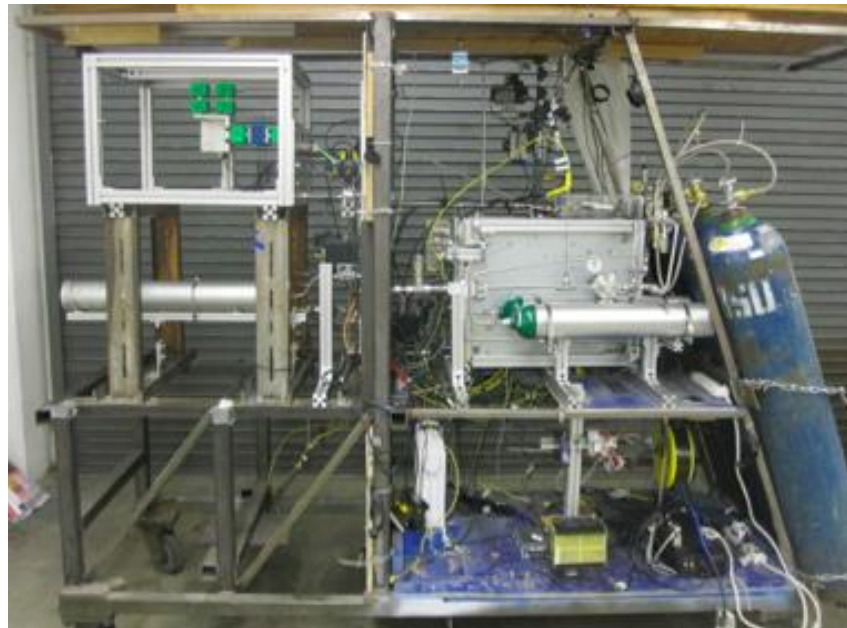


Figure 9. Ground Test Cart for TGALS LAPU Verification Testing.

³ <http://sine.ni.com/nips/cds/view/p/lang/en/nid/207535/>

CHAPTER 4

TESTING AND EVALUATION

A series of ground development tests using three different configurations were performed. First, cold flow valve tests were performed to characterize valve position versus voltage input. Next a series of static throttle position hot fire tests were performed to verify the throttle capability of the system using a cylindrical fuel port. After the system was decided to be ready, a helical port motor was printed and tested with static throttle positions to gather data about critical relationships between voltage input to the ball valve actuator and parameters such as chamber pressure, thrust, and mass flow rates. Once a basic closed loop controller was built, a series of short hot fire burns were performed to characterize system response for use in developing a simulation. This allowed determination of the optimal controller settings to match a given thrust profile. From the optimal controller settings, a final hot fire burn was performed to verify the simulation and system response.

4.1 Cold Flow Valve Characterization

In order to begin characterization of the ball valve and servo actuator, an open chamber was set up with a piece of phenolic with a .3” hole in place of a nozzle. At low pressure, a sweep of the ball valve was performed across its entire range of 0-5 volts, representing a range of 0-270 degrees. Figure 10 shows the results of the sweep test. The left graph represents the voltage command sent to the ball valve, and the right represents the calculated mass flow rate taking data from the differential pressure transducer attached to the venturi flow meter. The data gathered showed that the range of

interested for full closed to full open on the ball valve was in the range of 1V up to 2.7V. When performing the sweep tests, there is still an unknown amount of latency between giving the ball valve a command and the system responding.

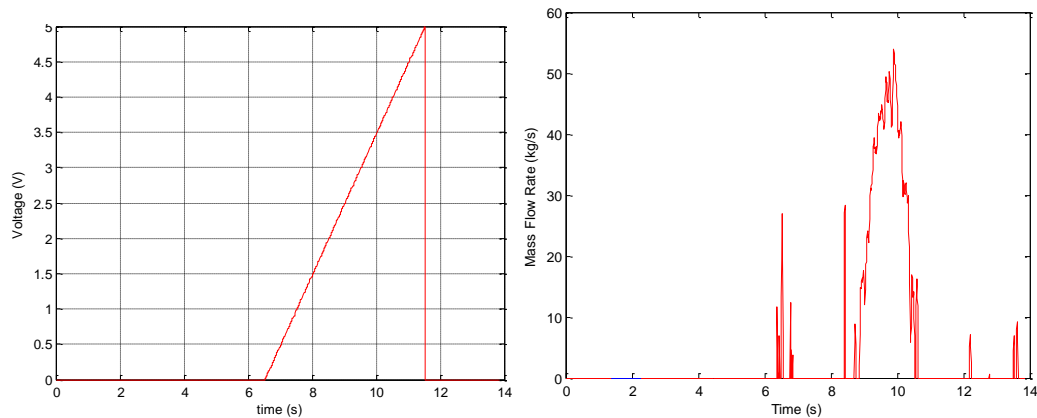


Figure 10. Cold Flow Sweep Mass Flow Data

Once a range of values was determined, static throttle position tests could be performed to narrow down true closed and open values for the ball valve without having to worry about latencies in the system. Figure 11 shows the results of the static throttle tests over a sweep of 1.2V to 2.6V. From this data it can be seen that a closed ball valve corresponds to a command of 1.1V and a full open command is 2.2-2.3V. In order to calculate the mass flows from the differential pressure transducer, the compressible Bernoulli equation is used. In order to verify that the venturi readings are correct, they are compared to choking mass flow, the maximum mass flow that can go through the

nozzle at the flow condition where velocity through the nozzle is at Mach 1. This is calculated by

$$\dot{m}_{ch} = \frac{A^* P_0}{\sqrt{T_0}} \sqrt{\frac{\gamma}{Rg} \left(\frac{2}{\gamma+1}\right)^{\frac{\gamma+1}{\gamma-1}}}, \quad (1)$$

where A^* is the nozzle area. The bounds in Figure 11 represent a range of C_d from .86 to 1, since it is unknown what the actual discharge coefficient of the sharp corner sonic phenolic nozzle is. The points that match correspond to a C_d of .93. The mass flow values calculated from venturi data seems reasonable.

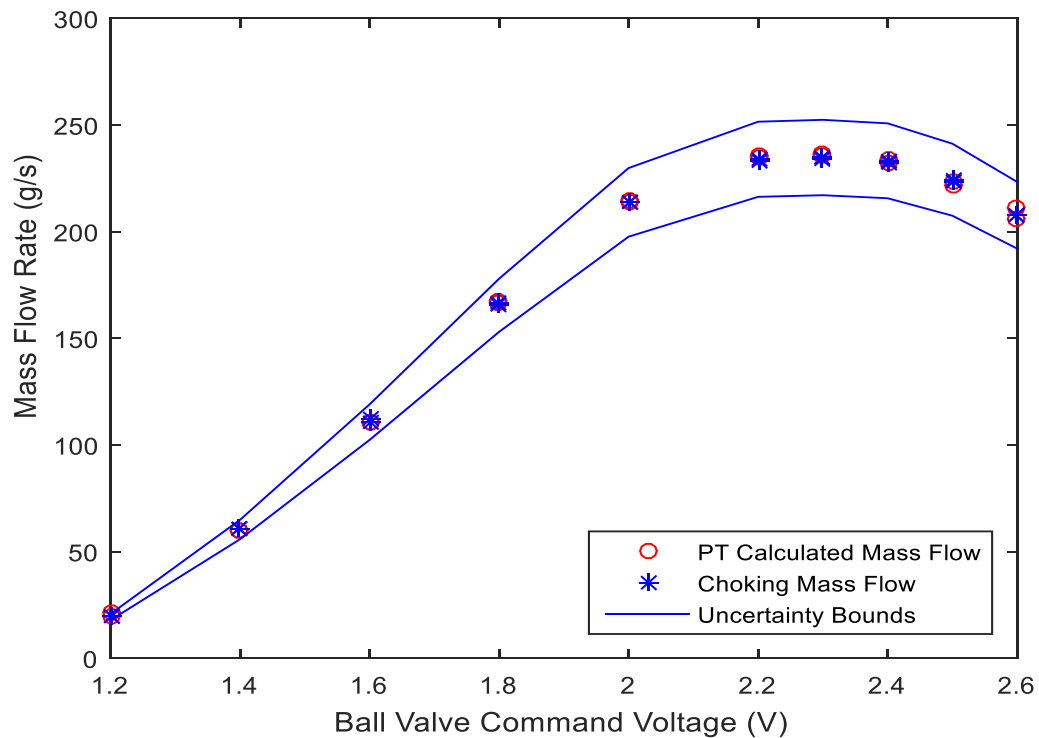


Figure 11. Static Throttle Position Results

4.2 Cylindrical Port Hot Fire Tests

The first series of hot fire ground tests were performed using an existing ABS fuel grain left over from earlier *nitrous oxide (N₂O)/ABS* testing campaign of Whitmore and Peterson. [33] Stratasys, Inc. printed this fuel grain as a single monolithic piece with a density of 0.975 g/cm^3 using a Fortus 900mc production FDM machine.⁴ This series of 5 tests were performed at the full throttle position with the ball valve set in the full opening position. Following each test, the motor fuel grain was removed from the motor case and the consumed fuel mass was measured.

Although real time thrust-stand oxidizer mass flow and motor mass measurements were obtained; for this testing campaign each grain was burned multiple times, and the motor disassembled after each test to allow intermediate mass measurements as a check on the accuracy of the real-time measurements. The fuel regression rate was calculated from the differences between the measured oxidizer and nozzle exit mass flows. The mean fuel port diameter calculated by simultaneously integrating the rate of regression.

$$\dot{r}_L = \frac{\dot{m}_{fuel}}{2\pi\rho_{fuel}r_L L} = \frac{\dot{m}_{total} - \dot{m}_{ox}}{2\pi\rho_{fuel}r_L L}. \quad (2)$$

Integrating Equation (2) from the initial condition to the current time solves for the longitudinal mean of the instantaneous fuel port diameter

$$r_L(t) = \sqrt{r_0^2 + \frac{1}{\pi\rho_{fuel}L} \int_0^t \dot{m}_{fuel} dt}. \quad (3)$$

⁴ <http://www.stratasys.com/3d-printers/production-series/fortus-900mc/>

Using the calculated longitudinal mean fuel port radius and the measured oxidizer mass flow rate (from the Venturi flow meter), the longitudinal mean of the oxidizer mass flux is estimated as

$$\bar{G}_{OX} = \frac{\dot{m}_{ox}}{\pi r_L^2}, \quad (4)$$

Figure 12 plots the measured resulting regression rates as a function of the oxidizer mass flux. (G_{ox}). For these calculations the oxidizer mass flow was measured using an in-line calibrated Venturi mass flow meter. The fuel mass flow was calculated as the difference between the measured oxidizer mass flow and the nozzle exit mass flow. The nozzle exit mass flow was calculated based on the measured chamber pressure P_0 , nozzle exit area A^* , and exhaust gas properties using the 1-dimensional de Laval choking mass flow equation, as shown above in equation 1. [34]

The combustion products for the combustion flame temperature T_0 , gas-specific constant R_g , and ratio of specific heats γ , were calculated using tables developed using the NASA chemical equilibrium program “Chemical Equilibrium with Applications,” (CEA). [35] For the CEA calculation the measured chamber pressure was used as an input, and the O/F ratio entered into CEA was adjusted to produce a fuel mass flow whose integral value exactly equaled the consumed fuel mass measured after each test.

Figure 12 also plots the best-fit exponential curve of the form

$$\dot{r}_L = a \cdot G_{ox}^n \cdot L^m, \quad (4)$$

where, \dot{r}_L is the mean longitudinal regression rate, $\{a\}$ is the scale factor, G_{ox} is the oxidizer mass flux, L is the fuel grain length, and $\{n, m\}$ are the burn exponents.

Assuming that $m=0$ removes any length effect upon the fuel regression rate. For a cylindrical fuel port with $m=0$, it can be shown that the oxidizer-to-fuel mass flow ratio (O/F) at any burn time is

$$O/F = \frac{1}{4^n \cdot \pi^{1-n}} \frac{\dot{m}_{ox}^{1-n} \cdot D_{port}^{2n-1}}{a \cdot \rho_{fuel} \cdot L}, \quad (5)$$

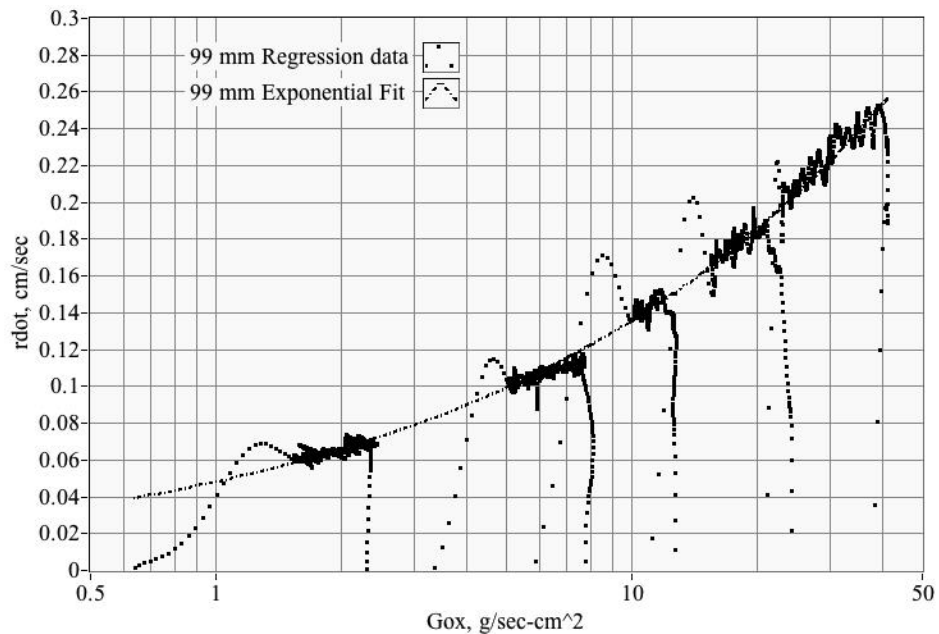


Figure 12. Regression Rate for GOX/ABS Cylindrical Port Tests.

Analysis of Eq. (2) shows that when the burn exponent is $\{n > 1/2\}$, the O/F ratio is progressive and increases as the fuel grain burns and the port opens up. Conversely, when $\{n < 1/2\}$ the O/F burn is regressive and becomes increasingly rich with time, and $\{n = 1/2\}$ the burn rate is neutral and implies no O/F shift during the burn. The majority of

commonly used oxidizer/fuel combinations (including N_2O/ABS) have burn exponents greater than $1/2$, and thus burn increasing leaner with time. [36]

For the GOX/ABS grain cylindrical fuel port tests, the resulting best-fit burn parameters are

$$\begin{bmatrix} a \\ n \end{bmatrix} = \begin{bmatrix} 0.048 \frac{cm^{2n+1}}{g-s^{1-n}} \\ 0.45 \end{bmatrix}, \quad (6)$$

The value for the burn exponent $\{n=0.450\}$ is considerably smaller than the value measured by Ref. (33), $\{n\sim 0.762\}$. The derived burn exponent suggests that the LAPU motor should exhibit very little O/F shift during the burn. Figure 13 verifies this assertion where O/F is plotted as a function of oxidizer mass flux.

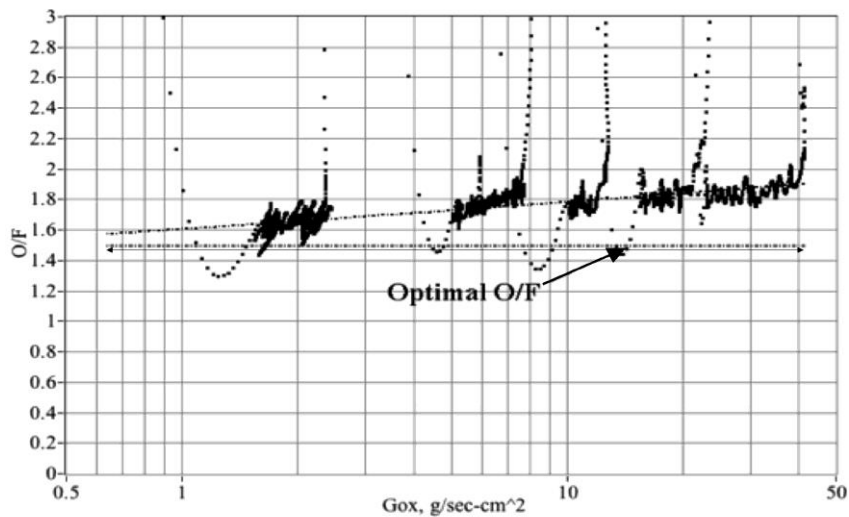


Figure 13. Oxidizer-to-Fuel Shift of Cylindrical ABS Fuel Port.

The *O/F* shift is slightly regressive with the motor burning only slightly richer as the fuel port opens up. This quantitative behavior matches the qualitative physical observations of the various motor burns. The larger 98-mm motor plume was observed to show very little change in the plume characteristics during the fuel grain burn lifetime -- approximate 20 seconds.

4.3 Measuring the Required Regulator Set Point

As shown by Fig. (11) the *O/F* ratios for the cylindrical port fuel grain lies just above the optimal operating value of approximately 1.5 for GOX/ABS. [37] Thus for the second series of tests a moderate helix was printed into the fuel grain to lower the mean *O/F* ratio. As listed in Table 1, the port helix radius was 1/2 of the initial fuel port diameter. The helix pitch length was 19.5 cm (7.68 in.) resulting in 3 complete turns along the fuel port length. This change was incorporated to slightly lower the *O/F* ratio so that the motor would burn nearer the optimal operating condition. The grain was printed as three interlocking segments on the MAE department's Dimension 1200es⁵ using ABSplus-340 feedstock. In addition to the modification of the fuel port, the nozzle retainer exhibited unwanted erosion, and a small redesign was made to reduce the erosion potential.

The testing campaign on the helical fuel port motor was broken into two sets. A primary function of the first test set was to measure the necessary regulator set point to achieve the full required 200 lbf thrust level. A series of 4, 2-second burns at various regulator set points were performed to determine the required level set pressure level. The

⁵ <http://www.stratasys.com/3d-printers/design-series/dimension-1200es/>

regulator output "droop" was found to be strongly a function of oxidizer mass flow.

Figure 14 plots these results. Fig. 14a plots regulator output from the set point (droop) as a function of the oxidizer mass flow, and Fig. 14b plots the achieved output pressure as a function of the regulator set point.

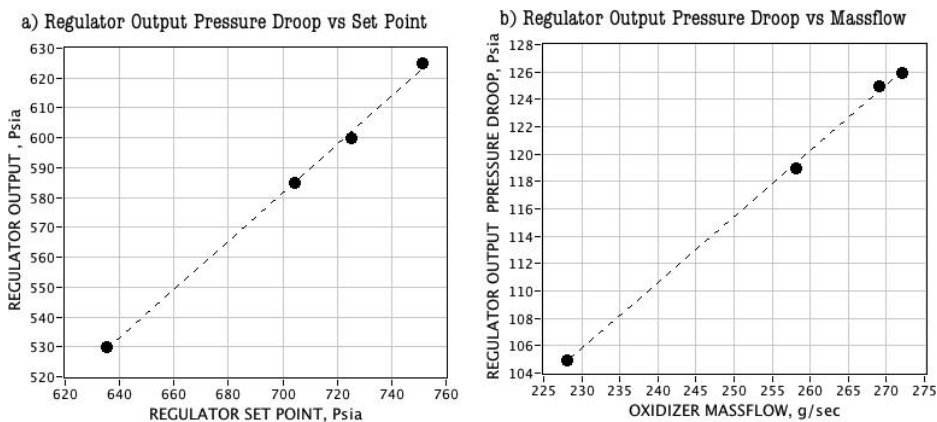


Figure 14. Regulator Droop as a Function of Oxidizer Mass Flow, Set Point.

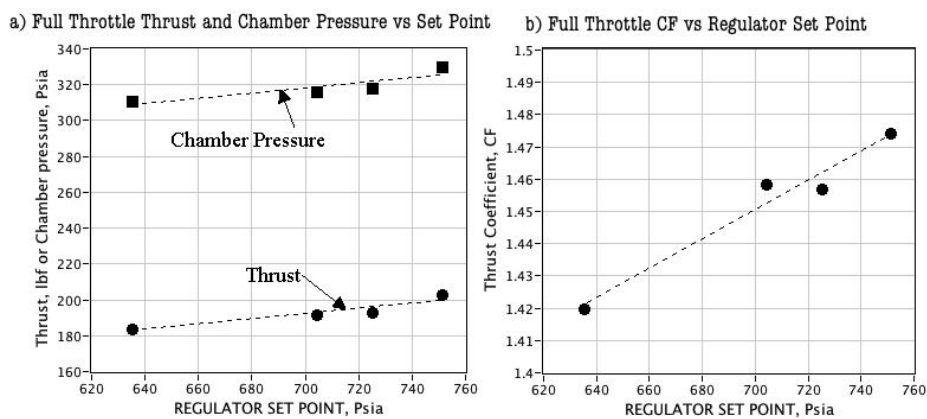


Figure 15. Full Throttle Thrust Chamber Pressure, and Thrust Coefficient as a Function of Regulator Set Point.

The result is that the achieved full-open thrust and chamber pressure are also strongly a function of the regulator set point. Thrust coefficient is also strongly influenced by the regulator set point. Figure 15 plots this result. With the throttle ball-valve fully open, the full required thrust level of 200 lbf mandates a regulator set point of at least 750 psig.

4.4 Oxidizer-to-Fuel Ratio for the Helical Fuel Port

The initial tests of the helical fuel port were also used to verify that the changes to the grain configuration moved the O/F ratio to the optimal operating range. Figure 16 presents these results. Here Figure 16a plots the mean O/F ratio for each burn is plotted as a function of the accumulated burn time on the motor. The resulting O/F range -- between 1.25 and 1.67 -- is overlaid onto the characteristic velocity plot C^* on Figure 16b. Here the achieved O/F range brackets the optimal performance range, thereby verifying the helix grain design.

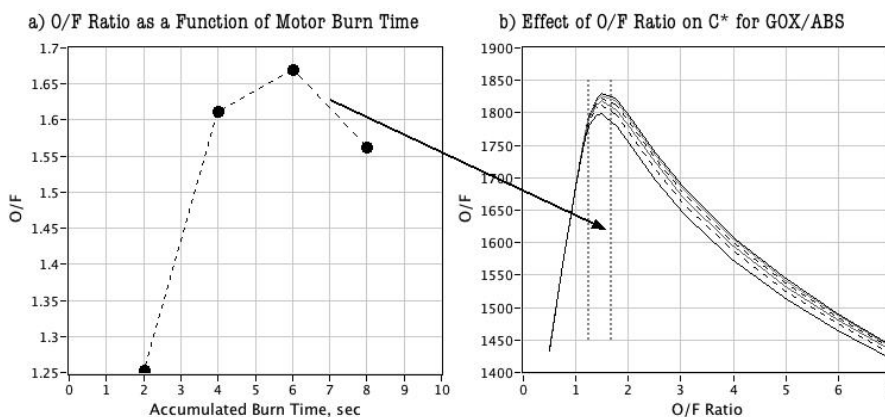


Figure 16. Achieved O/F Range for Helical Fuel Port Burn at Near Full Throttle and the resulting Effect on C^* .

Figure 17 compares the achieved C^* calculated by

$$C_{measured}^* = \frac{P_0 \cdot A^*}{\dot{m}_{total}}, \quad (4)$$

against the 100% combustion efficiency theoretical values for the O/F levels of Figure 16. Figure 17 also plots the measured combustion efficiency and specific impulse, I_{sp} .

The achieved combustion efficiencies, as calculated by Eq. 5, are slightly less than 80%.

$$\eta^* = \frac{C_{measured}^*}{C_{theoretical}^*}, \quad (5)$$

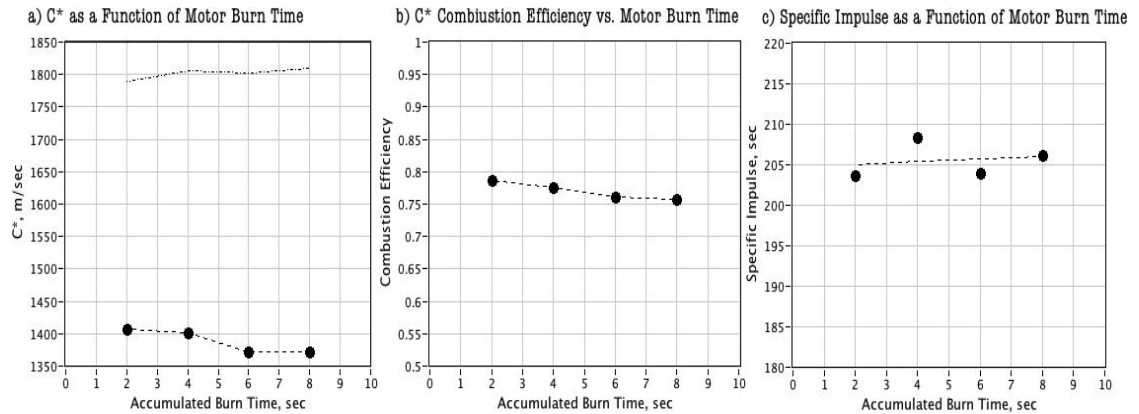


Figure 17. Cstar, Combustion Efficiency, and Isp as a Function of Burn Time. The low observed combustion efficiency is also reflected by the measured specific impulse of the system; which at a value of $I_{sp}=205$ seconds, is approximately 10% lower than predicted. The small drop in C^* is a result of a slight observed nozzle erosion during the 8-seconds of burn time. The reasons for the low observed performance levels have yet to be determined at this point. Two causes currently being investigated include an

incompletely cured printed fuel grain, and potential blow-by at the phenolic liner/graphite nozzle interface.

4.5 Throttle Curve Evaluation

Following the initial set of tests to determine the appropriate regulator set point, a series of six static throttle burns were performed at different ball valve voltage command levels, and using a newly fabricated helical fuel grain. To ensure that the fuel grain was fully cured, the newly printed grain was placed into a vacuum chamber, and then left in front of a fan overnight before performing these tests. Each burn was set as 2 seconds in length using up approximately 12 seconds of total burn lifetime.

Figure 18 summarizes the test results where the achieved motor thrust, mass flows, chamber pressure, and thrust coefficients are plotted as a function of the commanded ball valve voltage. Figure 18a also plots the required 200 lbf thrust full-throttle level. The effective range of the ball valve servo voltage command varies from 1.25 Volts (0% throttle) to 2.3 Volts (100% Throttle).

Figures 19 and 20 plot the system performance parameters including combustion efficiency and specific impulse as a function of the commanded throttle level and the equivalent throttle actuator voltage command. At full throttle, the system achieves slightly better combustion efficiency $> 80\%$ than was observed with the previous static tests; but this combustion efficiency and the associated specific impulse drops off significantly at the lower throttle levels. The plots of Figure 20 support the earlier assertion that the lower than predicted specific impulse for the system is a result of

lowered combustion efficiency.

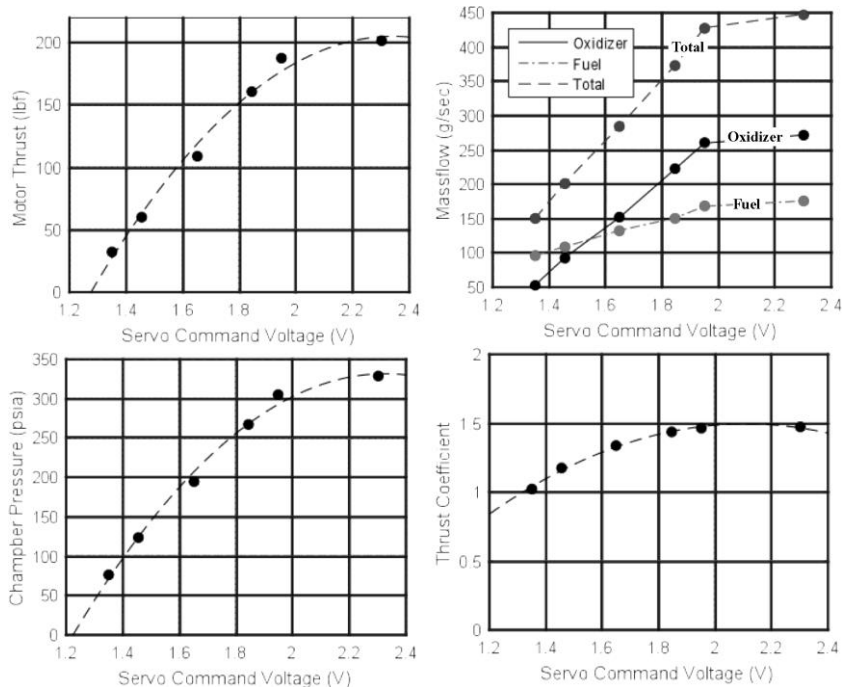


Figure 18. Helical Motor Response as Function of Commanded Ball Valve Voltage Level.

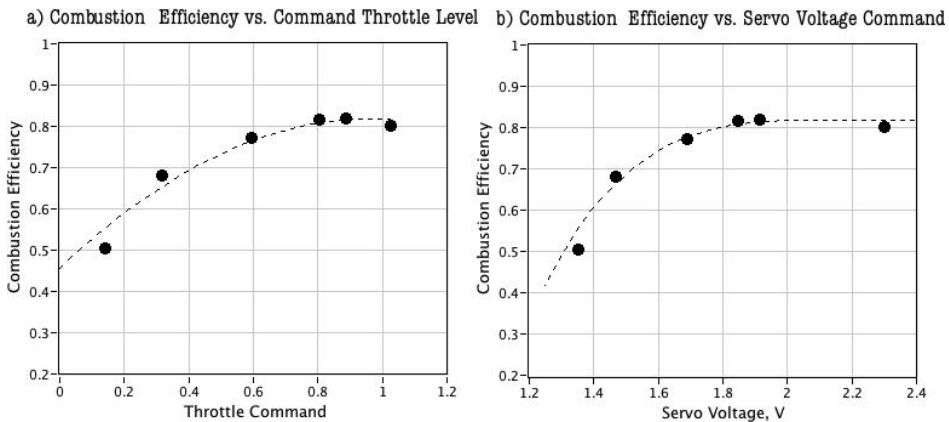


Figure 19. Combustion Efficiency as a Function of Throttle Command.

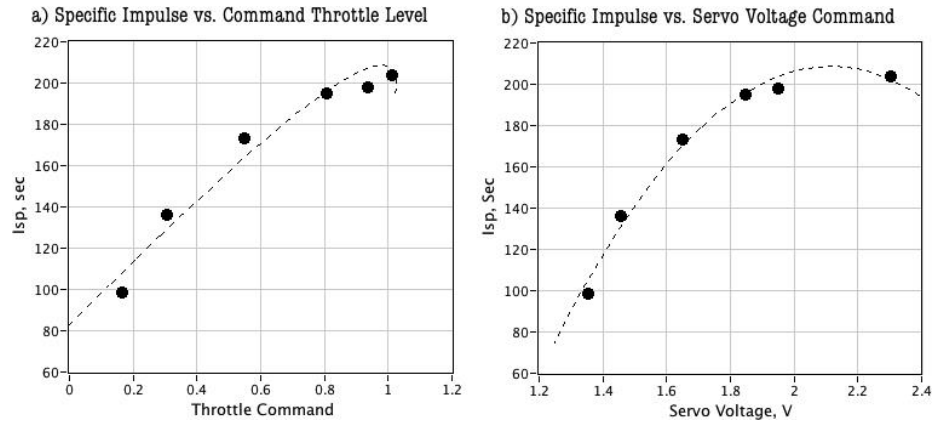


Figure 20. Specific Impulse as a Function of Throttle Command.

4.6 Closed Loop Throttle Testing

The results of the static throttle tests were curve fit and used to generate look-up tables that correlate the servo command voltage to motor thrust and chamber pressure to motor thrust. Using these data tables, a proportional-gain closed-loop controller using chamber pressure feedback was developed and implemented within the LabVIEW code that resides on the controlling laptop computer. Measured feedback data and closed-loop commands are sent to and from the *NI cDAQ-9174 Data Acquisition and Control Unit* via an amplified Universal Serial Bus (USB) extension.

The flow chart in Figure 21 shows the implemented filtered-proportional control law. The control features chamber pressure feedback with closed loop servo-voltage output commands. An option for smoothing the commanded voltage using a second order Butterworth filter is included. Options for user-prescribed thrust profile inputs are available, including step, ramp, and pull-up push-over maneuver. Values for the proportional gain k_p and Butterworth filter cutoff frequency ω_p , are user inputs.

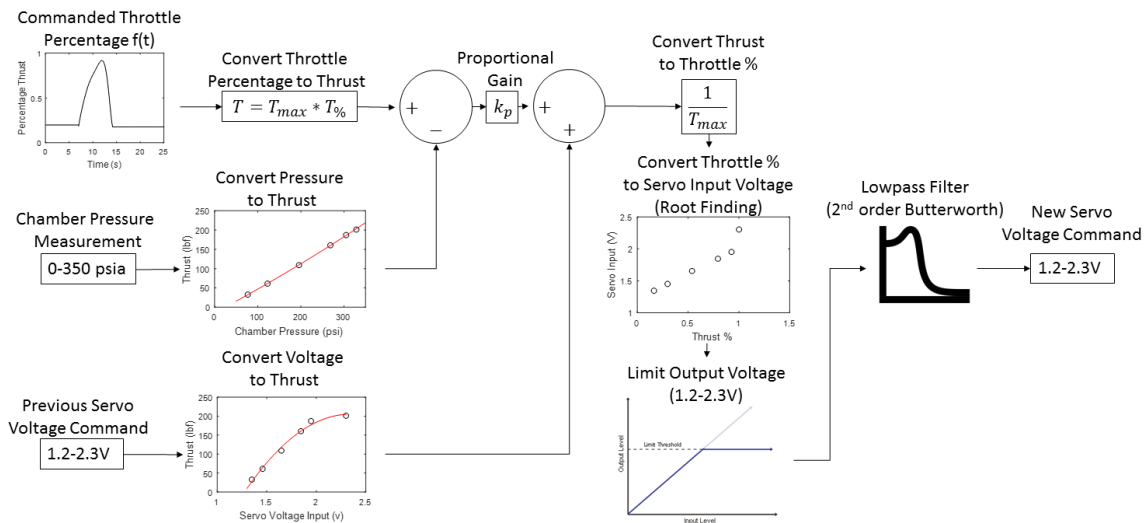


Figure 21. Proportional Closed-Loop Controller Layout.

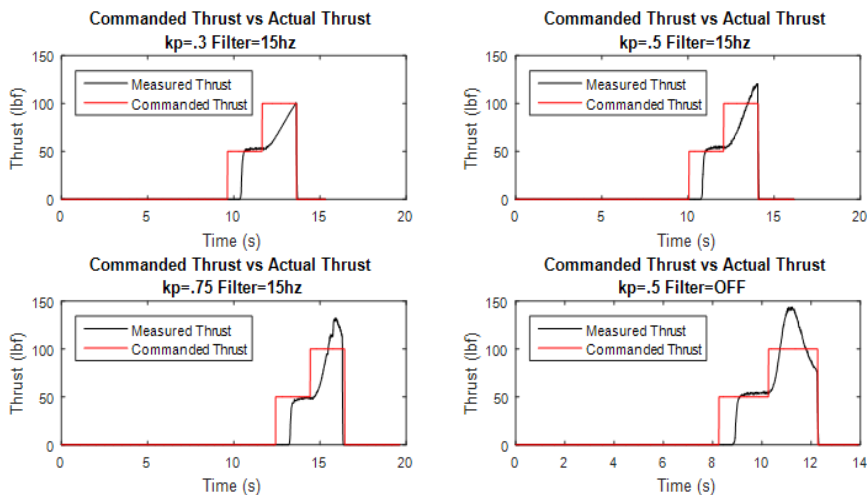


Figure 22. Thrust Profiles for Various Closed-Loop Step Tests.

Figure 22 shows the result of a 4 hot-fire tests performed with various set values for k_p and ω_p . For these tests the motor was ignited with the actuator command set for the

25% thrust (50 lbf) level, and the commanded thrust was increased to 50% (100 lbf) 2 seconds into the burn. The lowest gain $k_p = 0.3$ and a command filter cutoff frequency of $\omega_p = 94 \text{ radians/sec}$ (15 Hz) produced the response with the minimal overshoot. The observed response latency is primarily a function of the actuator response time.

4.7 Closed Loop Throttle Filter Tuning

Using the controller command logic from the closed loop step tests, a simulation was designed so that ω_p and k_p can be "tuned" without requiring multiple trial-and-error hot-fire tests. The simulation decomposes the system dynamics into two concatenated components 1) a model of the servo and control ball valve dynamics, and 2) a model of the ballistic response of the motor combustion chamber. Both responses are modeled as second order transfer functions. The ball servo and ball valve transfer function is

$$\frac{\%MVT}{V_{cmd}} = \frac{1}{\left(\frac{\tau_1}{2\zeta_1}\right)^2 \cdot s^2 + \tau_1 \cdot s + 1} = \frac{\omega_{n1}^2}{s^2 + 2\zeta_1 \omega_{n1} \cdot s + \omega_{n1}^2}, \omega_n = \frac{2\zeta_1}{\tau_1}, \quad (6)$$

where $\{\tau_1 = 0.52\}$ and $\{\zeta_1 = 0.85\}$, and ω_{n1} is the natural radian frequency of the combined servo/ball valve system. These values are based on Invenscience® specifications⁶ for the servo response properties. In Eq. (6) $\%MVT$ is the percentage of mean valve travel from fully closed to fully open -- approximately 90 degrees, and V_{cmd} is the servo command voltage level. The motor ballistics transfer function relating thrust F to percentage of valve travel $\%MVT$ is modeled by a simple second order linear system

⁶ http://www.invenscience.com/index_files/torxis_rotary_servo.htm/

$$\frac{F}{\%MVT} = \frac{1}{\left(\frac{\tau_1}{2\zeta_2}\right)^2 \cdot s^2 + \tau_2 \cdot s + 1}, \quad (7)$$

where the values for the time lag $\{\tau_2\}$ and damping ratio $\{\zeta_2\}$ are calculated to give the minimum-variance fit between the simulator and measured response. Figure 23 shows the calculation sequence that was used to estimate the best-fit transfer functions. For a given control law parameter setting for ω_p and k_p , the simulation was run multiple times, sweeping through the 2-dimensional parameter space for $\{\tau_2, \zeta_2\}$. In this two-dimensional parameter space, the parameter set that produces the minimum root-sum-square (RSS) error between the measured system and simulation response is selected as the "best-fit" for the motor ballistics.

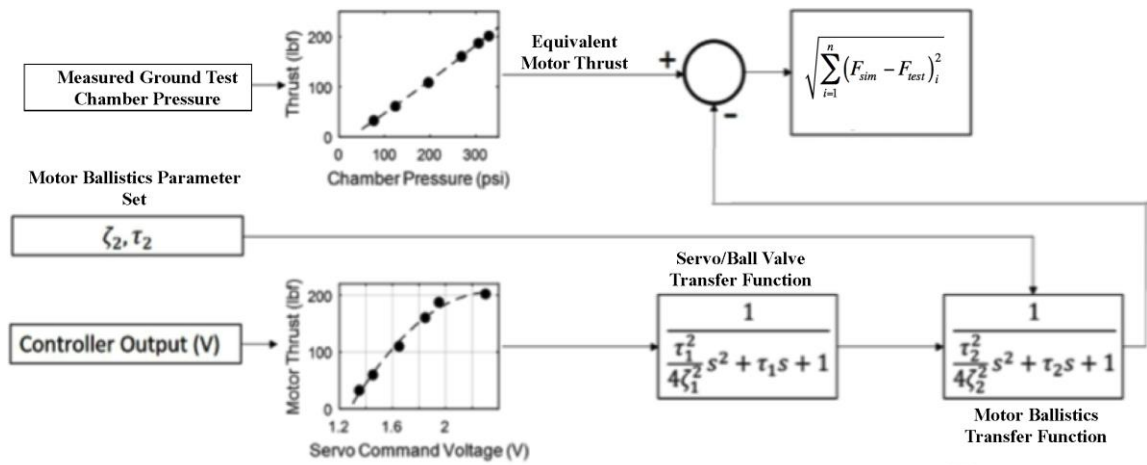


Figure 23. Finding the Best Fit Transfer Function Parameters.

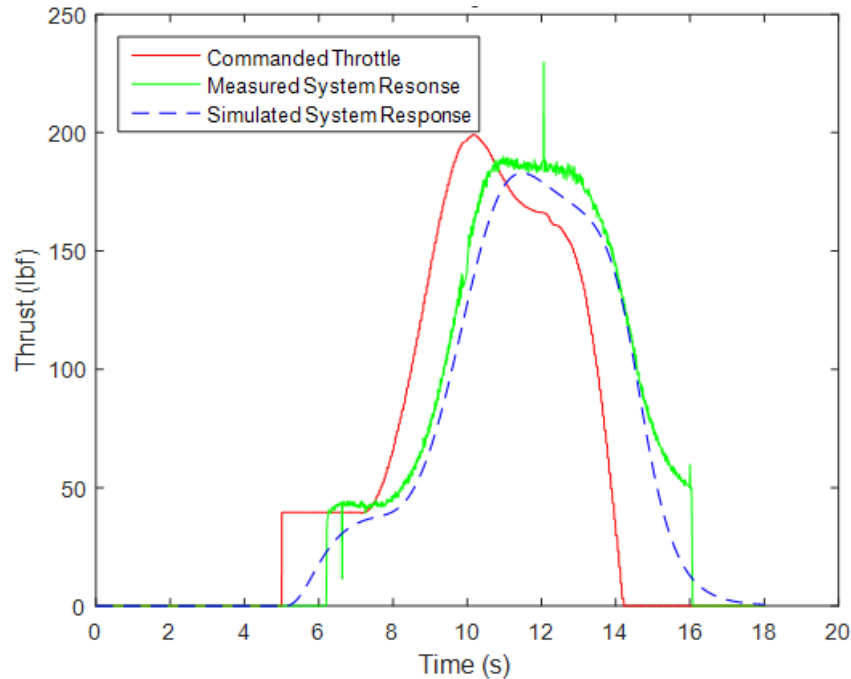


Figure 24. Simulation Matching for Full Length Hot-Fire Test

Figure 24 shows the RSS best-fit comparison between the simulation and hot-fire test data for a prescribed throttle profile corresponding to a pull-up push-over maneuver of the TGALS vehicle. [38] For this fit, the simulation best matched when $\{\tau_2 = 0.7 \text{ and } \zeta_2 = 1.9\}$.

Using this transfer function parameter set for the ballistic model, various values of the control law parameter set $\{\omega_p \text{ and } k_p\}$ were evaluated, and allowed the control law to be tuned for a best system response. Figure 25 shows a sample of various simulation runs and illustrates the effects of the control law parameter set. The control law parameters weren't just selected to give the best response; they were chosen to best imitate the pull-up push-over maneuver's thrust profile, even if that meant a slightly higher latency in the throttle response.

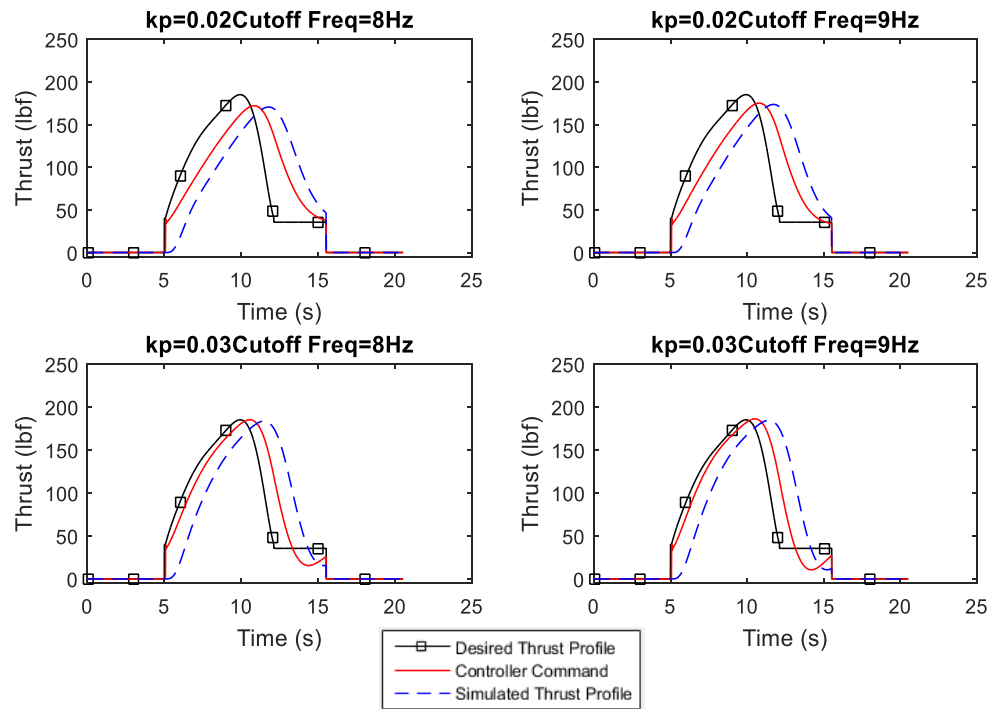


Figure 25. Sample Controller Tuning Simulation Runs

4.8 Closed Loop Throttle Following Tests

Due to discrepancies between the simulated and physical systems, two attempts at following the pull-up push-over maneuver throttle profile were made before the third test matched what was expected from the simulation. This allowed for repetition of the above steps to verify that the selected transfer functions correctly modelled the system. Figure 26 shows the thrust profile of the successful throttle following test in green, compared to the predicted value from the simulation shown as a dashed blue line, where the black line is the thrust profile desired for the pull-up push-over maneuver as defined by NASA Armstrong. The profile matching the predicted thrust from the simulation proves that the system model is accurate enough to simulate system response, and allow for system

tuning without the necessity for large numbers of hot fire tests. The chosen values were simply to show that the system could be correctly modelled, and don't necessarily represent the best possible response case.

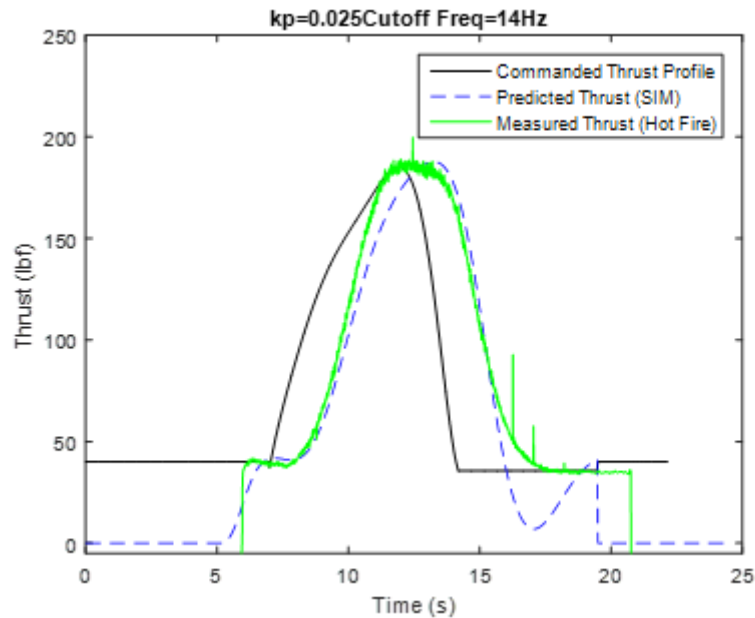


Figure 26. Verification Push-up Pull-over Thrust Profile

4.9 Commanded Thrust Profile to Response Transfer Function

The final step desired was to have a transfer function relating the commanded thrust profile to the measured thrust value for use with in house simulations to verify the thrust response is sufficient to meet mission requirements. The same method as above in Section 4.7, Figure 23 was implemented with only a single second order transfer function relating the commanded thrust profile to the measured thrust, instead of the controller command thrust to the measured thrust as was done above. The second order system for this case is

$$\frac{F}{F_{cmd}} = \frac{1}{\left(\frac{\tau}{2\zeta}\right)^2 \cdot s^2 + \tau \cdot s + 1}, \quad (8)$$

Figure 27 shows the best fit transfer function found using this method. For $\tau = 1.29, \zeta = 0.62$ the simulation (blue) is shown transposed over the measured thrust (green) given the commanded thrust (black).

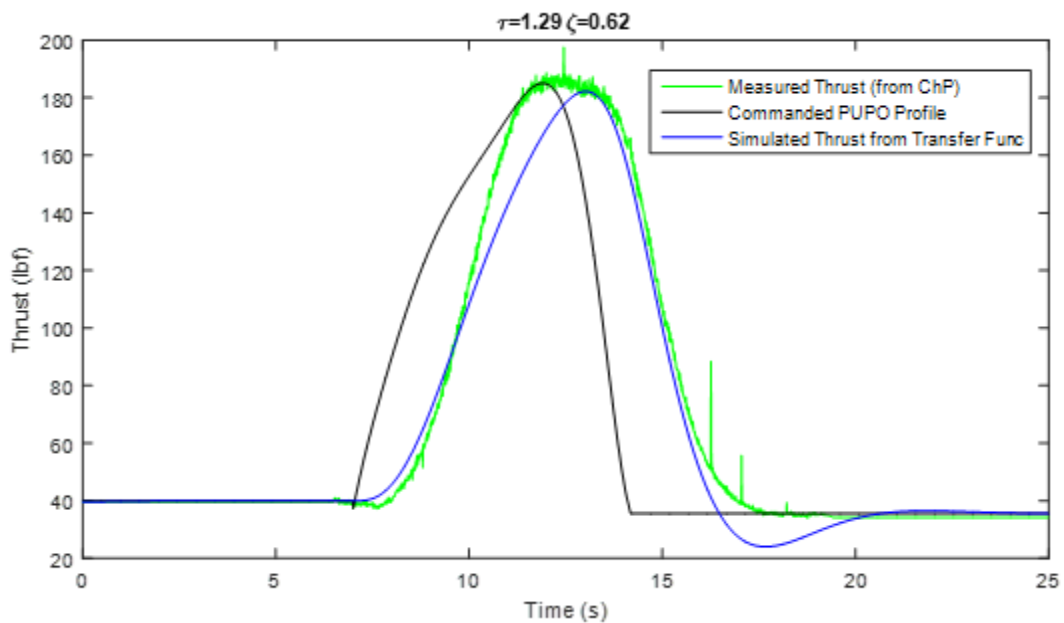


Figure 27. Best Fit Transfer Function Commanded Thrust to Measured Thrust

CONCLUSION

This document presents a status update of the design and integration of a throttled launch assist hybrid rocket motor for an airborne nano-launch platform. Currently, NASA Armstrong Flight Research Center is developing a scaled prototype of a high lift-to-drag ratio glider designed as a flexible low earth orbit launch platform for nano-scale satellites. Because the high L/D platform is delivered to the launch altitude and airspeed using a high-efficiency air-breathing propulsion system, there is a significant reduction in the required ΔV that must be delivered by the launch vehicle. Optimal ΔV savings are achieved when the NanoSat launch vehicle is delivered to a high-flight path angle that will approximate the condition that would be achieved along a ground launch trajectory at the same altitude and airspeed.

The glider platform itself is unable to achieve this flight condition, and launch assist propulsion is required. A hybrid system was selected for the launch assist motor because of the inherent safety, operational simplicity, and environmental friendliness of the propellants; and because of the ability for the hybrid system to be throttled and restarted on demand. This study establishes the requirements for this launch assist propulsion system, develops the system design features, presents the end-to-end hardware layout, develops the closed-loop throttle control law, develops the simulation used to tune control parameters, and shows the result of hot fire when using the best picked closed loop controller parameters.

A closed loop, proportional control system is utilized to generate a voltage output command for throttling purposes. An option to have a second order Butterworth filter to smooth the output voltages is available. Options for user-prescribed thrust profile inputs are available, including step, ramp, and pull-up push-over maneuver. Values for the proportional gain the Butterworth filter cutoff frequency are user selectable. A medium fidelity motor simulation is derived from preliminary ground test data and is used to tune the parameters of the closed-loop control law without having to perform multiple hot-fire tests.

Initial static tests were performed with a cylindrical fuel port to verify system functionality and establish a baseline for the propellant regression rate and optimal O/F ratio. Subsequent tests are performed using a helical fuel port to increase the volumetric efficiency of the system and allow operation near the optimal oxidizer-to-fuel condition. Multiple restarts of each system configuration are demonstrated. Results of both open and closed loop throttle tests are presented.

Static throttle tests were curve fit and used to generate look-up tables that correlate the servo command voltage to motor thrust and chamber pressure to motor thrust. Using these data tables, a proportional-gain, closed-loop controller using chamber pressure feedback was developed and implemented within the real-time code that resides on the controlling laptop computer. Closed loop system tuning has been completed for the current iteration of the ground test. Follow-on work will consist of integrating the system onto the glider pylon and modifying the control code for the chosen flight computer.

Ground testing for the integrated system will be performed, and once any remaining safety checks have been passed, the system will be ready for flight.

REFERENCES

- [1] Bartolotta, P., Wilhite, A. W., Schaeffer M., Volland, R. T., and Huebner, L., " Horizontal Launch: A Versatile Concept for Assured Space Access," NASA/SP-2011-21599, December 2011.
- [2] Lanre, A. M., Fashanu, T. A., and Osheko, A. C., " Parameterization of Micro Satellite Launch Vehicle," J. Aeronautics and Aerospace Engineering, Vol. 3, No. 2, February 2014., <http://dx.doi.org/10.4172/2168-9792.100013>.
- [3] Hague, N. Capt., Siegenthaler, E., Lt. Rothman, J., "Enabling Responsive Space: F-15 Microsatellite Launch Vehicle", AIAA J. of Spacecraft and Rockets, IEEEAC paper # 1102, December 2002, https://wiki.umn.edu/pub/AEM_Air_Launch_Team/Aircraft/Enabling_responsive_space-F-15_microsatellite_launch_vehicle.pdf
- [4] Chen, T. T., Ferguson, P. W., " Responsive Air Launch Using F-15 Global Strike Eagle," RS4-2006-20014th Responsive Space Conference, Los Angeles CA, April 24-27, 2006.
- [5] Anon, "Hazard Analysis of Commercial Space Transportation; Vol. 1: Operations, Vol. 2: Hazards, Vol. 3: Risk Analysis," U.S. Dept. of Transportation, PB93-199040, Accession No. 00620693 , May 1988.
- [6] Altman, D., "Hybrid Rocket Development History," *27th AIAA, SAE, ASME, and ASEE, Joint Propulsion Conference*, 1991.
- [7] Cheng, C. G., Farmer, R. C., Jones, H. S., and McFarlane, J. S., "Numerical Simulation of the Internal Ballistics of a Hybrid Rocket," AIAA Paper 94-0554, [30th AIAA/ASME /SAE/ASEE Joint Propulsion Conference & Exhibit, Indianapolis, IN July, 1994.]
- [8] Anon., "Department of Defense Interface Standard, Electromagnetic Environmental Effects requirements for Systems, MIL-STD-464, [http:// www.tscm.com/MIL-STD-464.pdf](http://www.tscm.com/MIL-STD-464.pdf), [Retrieved 8 October 2012].
- [9] Anon., "Weapons Systems and Platforms (WP) Focus Area. Environmentally Friendly Sustainable Binder System for Energetic Materials," 2014 Strategic Environmental Research and Development Program (SERDP), Exploratory Development (SEED) BAA-13-0002. This proposal responds specifically to FY2014 SEED Statement of Need, WPSEED-14-01.
- [10] Whitmore, S. A., Peterson, Z. W., and Eilers, S. D., "Comparing Hydroxyl Terminated Polybutadiene and Acrylonitrile Butadiene Styrene as Hybrid Rocket Fuels," AIAA J. Propulsion and Power, vol. 29, no. 3, May–June 2013.

- [11] Whitmore, S. A., Walker, S. D., Merkley, D. P., and Sobbi, M. "High Regression Rate Hybrid Rocket Fuel Grains with Helical Port Structures", *Journal of Propulsion and Power*, Vol. 31, No. 6 (2015), pp. 1727-1738. DOI: 10.2514/1.B35615
- [12] Whitmore, S. A., Inkley, N. R., Merkley, D. P., and Judson, M. I., "Development of a Power-Efficient, Restart-Capable Arc Ignitor for Hybrid Rockets", *Journal of Propulsion and Power*, Vol. 31, No. 6 (2015), pp. 1739-1749. DOI: 10.2514/1.B35595
- [13] Moore, G. E. and Berman, K., "A Solid-Liquid Rocket Propellant System," *Jet Propulsion*, Vol. 26, No. 11, November 1956, pp. 965–968.
- [14] Duban, P., "The "LEX" rocket probe (LEX small rocket probe for in-flight testing of ONERA studies of hybrid propulsion, discussing design and program)," *L'Aeronautique et L'Astronautique*, 1968, pp. 47–54.
- [15] Mead, F. B., Bornhorst, B. R. and J., "Certification Tests of a Hybrid Propulsion System for the Sandpiper Target Missile," *AFRPL-TR- 69 -73*, 1969.
- [16] Jones, R. A., "Hybrid Propulsion System for an Advanced Rocket-Powered Target Missile," *Quarterly Technical Report, UTC2220-QTR2*, 1967.
- [17] Penn, C. D. and Branigan, J. E., "Preliminary Flight Rating Tests of the HAST Propulsion System," *AFRPL-TR-15-5*, 1975.
- [18] Hamers, J., "Experimental Investigation of Prepackaged Hybrid Propellant Systems," *Final Report AFRPL-TR-67-168*, 1967.
- [19] Sutton, G. P. and Biblarz, O., *Rocket Propulsion Elements, 7th Ed.*, Wiley, New York City, NY, 2001.
- [20] Flittie, K. J., Estey, P. N., and Kniffen, R., "The Aquila Launch Vehicle: A Hybrid Propulsion Space Booster," *Acta Astronautica*, Vol. 28, 1992, pp. 99–110.
- [21] Boardman, T. A., Carpenter, R. L., Goldberg, B. E., and Shaeffer, C. W., "Development and Testing of 11- and 24-inch Hybrid Motors under the Joint Government/Industry IR&D Program," *AIAA Paper 93-2552*, 1993.
- [22] Carpenter, R. L., Boardman, T. A., Claflin, S. E., and Harwell, R. J., "Hybrid Propulsion for Launch Vehicle Boosters: A Program Status Update," *31st AIAA/ASME/SAE/ASEE Joint Propulsion Conference and Exhibit, San Diego CA*, July 10-12, 1995.
- [23] Arves, J., Gnau, M., Joiner, K., Kearney, D., McNeal, C., and Murbach, M., "Overview of the Hybrid Sounding Rocket (HYSR) Project." *AIAA 2003-5199*, 2003.
- [24] Wright, A. B., Teague, W., Wright, A. M., and Wilson, E. W., "Instrumentation of UALR Labscale Hybrid Rocket Motor," *Proc. of SPIE*, Vol. 6222, 2006.

- [25] Dyer, J., Doran, E., Dunn, Z., Lohner, K., Bayart, C., Sadhwani, A., Zilliac, G., Cantwell, P. B., and Karabeyoglu, A., "Design and Development of a 100 km Nitrous Oxide/Paraffin Hybrid Rocket Vehicle," *AIAA 2007-5362*, 2007.
- [26] Doran, E., Dyer, J., Marzona, M. T., Karabeyoglu, A., Zilliac, G., Mosher, R., and Cantwell, B., "Status Update Report for the Peregrine Sounding Rocket Project: Part III," *AIAA 2009-4840*, 2009.
- [27] Austin, B., Heister, S., Dambach, E., Wernimont, E., and Meyer, S., "Variable Thrust, Multiple Start Hybrid Motor Solutions for Missile and Space Applications," *46th AIAA/SME/SAE/ASEE Joint Propulsion Conference, Nashville TN*, July 25-28, 2010.
- [28] Whitmore, S. A., Walker, S. D., Merkley, D. P., and Sobbi, M. "High Regression Rate Hybrid Rocket Fuel Grains with Helical Port Structures", *AIAA J. Propulsion and Power*, Vol. 31, No. 6 (2015), pp. 1727-1738.
- [29] Whitmore, S. A., Inkley, N., and Merkley, D. P., "Development of a Power-Efficient, Restart-Capable Arc Ignitor for Hybrid Rockets", *AIAA J. Propulsion and Power*, Vol. 31, No. 6 (2015), pp. 1739-1749.
- [30] Anon., "Department of Defense Interface Standard, Electromagnetic Environmental Effects Requirements for Systems," MIL-STD-464, <http://www.tscm.com/MIL-STD-464.pdf> [Retrieved 8 October 2014].
- [31] Anon., "High Power 8C-30C Series, Single Output High Voltage DC/DC Modules," UltraVolt, Inc., http://www.ultravolt.com/uv_docs/HP8C-30CDS.pdf, [Retrieved 9 October 2014].
- [32] Whitmore, S. A., Merkley, S. L., Walker, S. D., Tonc, L., Spurrier, Z. S., and Mathias, S., "Survey of Selected Additively Manufactured Propellants for Arc-Ignition of Hybrid Rockets," *AIAA 2015-2616, 51st AIAA/ASME/SAE/ASEE Joint Propulsion Conference and Exhibit*, Orlando FL, 27-29 July, 2015.
- [33] Whitmore, S. A., Peterson, Z. W., and Eilers, S. D., "Comparing Hydroxyl Terminated Polybutadiene and Acrylonitrile Butadiene Styrene as Hybrid Rocket Fuels," *AIAA J. Propulsion and Power*, vol. 29, no. 3, May–June 2013.
- [34] Sutton, G. P., and Biblarz, O., *Rocket Propulsion Elements*, 7th ed., Wiley, New York, 2001, Chaps 4-5.
- [35] Gordon, S., and McBride, B. J., "Computer Program for Calculation of Complex Chemical Equilibrium Compositions and Applications," NASA RP-1311, 1994.
- [36] Karabeyoglu, A., "Lecture 10 Hybrid Rocket Propulsion Design Issues," AA 284a Advanced Rocket Propulsion, AAE Department, Stanford University, May 14, 2012, p. 18, http://www.spg-corp.com/docs/Stanford_AA284a_Lecture10.pdf, [Retrieved 01 January, 2016].

- [37] Whitmore, S. A., Walker, S. D., Merkley, D. P., and Sobbi, M. "High Regression Rate Hybrid Rocket Fuel Grains with Helical Port Structures", *AIAA J. Propulsion and Power*, Vol. 31, No. 6 (2015), pp. 1727-1738.
- [38] Whitmore, S. A., Merkley, S. L., Walker, S. D., and Spurrier, Z. S. "Throttled Launch-Assist Hybrid Rocket Motor for an Airborne NanoSat Launch Platform", 51st AIAA/SAE/ASEE Joint Propulsion Conference, Propulsion and Energy Forum, (AIAA 2015-3940), 28-30 July 2015, <http://dx.doi.org/10.2514/6.2015-3940>.